8

Continuous-time impurity solvers

This chapter, like the previous one, describes quantum Monte Carlo methods for the simulation of a system of interacting electrons at nonzero temperature. Here, we target a particular class of problems, characterized by a small number of correlated sites or orbitals, that we call impurity problems. While we could apply the methods of the previous chapter to such impurity models, the algorithms discussed here are more advantageous not only because they work in continuous imaginary time and hence lack the Trotter approximation error inherent to the previous methods, but also because they manipulate determinants of matrices of smaller size, which can be handled more efficiently. At the same time, the continuous-time approach is applicable to broader classes of impurity problems.

Driving the development of these continuous-time impurity solvers was the desire to perform more efficient simulations of correlated lattice models within the framework of dynamical mean-field theory. This formalism maps the lattice problem onto an impurity problem, whose parameters are determined by a self-consistency condition. In some cases, the self-consistent solution gives a good approximation of the properties of the original lattice problem. When we combine this dynamical mean-field approximation with the local-density approximation for electronic structure calculations, we obtain a powerful scheme for electronic structure calculations of strongly correlated materials. In this chapter we discuss the most important classes of impurity models, sketch the basics of the dynamical mean-field approximation, and detail the different variants of continuous-time impurity solvers.

8.1 Quantum impurity models

A quantum impurity model describes an atom or molecule embedded in some host with which it exchanges electrons, spin, and energy. This exchange allows the

https://doi.org/10.1017/CBO9780511902581.009 Published online by Cambridge University Press

impurity to make transitions between different quantum states, and in the presence of interactions within or between the impurity orbitals, these transitions lead to nontrivial dynamical properties. Quantum impurity models play a prominent role, for example, in the theoretical description of the magnetic and electric properties of dilute metal alloys and in theoretical studies of quantum dots and molecular conductors. These models also appear as an auxiliary problem whose solution yields the *dynamical mean-field* description of correlated lattice models.

The iconic impurity models are the single orbital Anderson impurity model

$$H = \sum_{k\sigma} \epsilon_k n_{k\sigma} + \sum_{k\sigma} \left(V_{k\sigma} c^\dagger_{k\sigma} d_\sigma + V^*_{k\sigma} d^\dagger_\sigma c_{k\sigma} \right) + \epsilon_d \sum_\sigma n_{d\sigma} + U n_{d\uparrow} n_{d\downarrow} \tag{8.1}$$

and the Kondo impurity model

$$H = \sum_{k\sigma} \epsilon_k n_{k\sigma} + \sum_{kk'} J_{kk'} \vec{S}_{kk'} \cdot \vec{s}. \tag{8.2}$$

In the original context, ϵ_k is the energy dispersion of a conduction electron of Bloch momentum k and spin σ (creation operator $c^\dagger_{k\sigma}$, $n_{k\sigma} = c^\dagger_{k\sigma} c_{k\sigma}$). In the Anderson impurity model the $V_{k\sigma}$ describe the hybridization of an electron in an impurity state (creation operator $d^\dagger_\sigma$, $n_{d\sigma} = d^\dagger_\sigma d_\sigma$) with those in the conduction band. The impurity level energy is ϵ_d, and a repulsive Coulomb energy U acts if two electrons occupy this level simultaneously. In the Kondo impurity model, the impurity is a localized quantum spin $\vec{s}$ coupled to the spin of the conduction band,

$$S^\alpha_{kk'} = \frac{1}{2} \begin{pmatrix} c^\dagger_{k\uparrow} & c^\dagger_{k\downarrow} \end{pmatrix} \sigma^\alpha \begin{pmatrix} c_{k'\uparrow} \\ c_{k'\downarrow} \end{pmatrix}.$$

Here, σ^α with $\alpha = x$, y, and z are the Pauli spin matrices, and the coupling is via a wave-number-dependent exchange interaction $J_{kk'}$. These two models were the subjects of decades of numerical and analytical attacks that resulted in an understanding of the Kondo effect. The properties of these models and their generalizations are still of considerable interest.

A canonical transformation (Section 9.2.2), called the Schrieffer-Wolff transformation, shows that the physics of the Anderson impurity model and Kondo impurity model are equivalent when the hybridization is weak, the impurity level is below the conduction band, and the Coulomb energy is the dominant energy scale. These conditions combine to restrict the electron occupation of the impurity to one electron. The Kondo exchange interaction is antiferromagnetic and roughly equals the momentum average of the square of the band energy divided by the Coulomb energy.

While these iconic models allow us to address general theoretical issues, they are somewhat unrealistic. Impurities (e.g., transition metal atoms) typically have

multiple orbitals. While generalizations to such situations are easily made, and simulations of such models with the determinant method of Chapter 7 have occurred (e.g., Bonča and Gubernatis, 1993a, 1994), the desire to treat more complex models generated a need for more efficient and more flexible impurity solvers.

The Hamiltonian of a general impurity model has the form

$$H = H_{\rm loc} + H_{\rm bath} + H_{\rm mix}, \tag{8.3}$$

where $H_{\rm loc}$ describes the impurity, characterized by a small number of degrees of freedom (typically spin and orbital degrees of freedom denoted by a, b, ...), and $H_{\rm bath}$ describes an infinite reservoir of free electrons, labeled by a continuum of quantum numbers p, and a discrete set of quantum numbers ν (typically spin). Finally, $H_{\rm mix}$ describes the exchange of electrons between the impurity and the bath in terms of hybridization amplitudes $V^a_{p\nu}$. Explicitly, the three terms are

$$H_{\rm loc} = \sum_{ab} \epsilon^{ab} d^\dagger_a d_b + \frac{1}{2} \sum_{abcd} U^{abcd} d^\dagger_a d^\dagger_b d_c d_d, \tag{8.4}$$

$$H_{\rm bath} = \sum_{p\nu} \varepsilon_p c^\dagger_{p\nu} c_{p\nu}, \tag{8.5}$$

$$H_{\rm mix} = \sum_{pa\nu} \left[V^a_{p\nu} d^\dagger_a c_{p\nu} + (V^a_{p\nu})^* c^\dagger_{p\nu} d_a \right]. \tag{8.6}$$

Note that in this general context, the bath energies ε_p can be arbitrary; that is, they are not necessarily related to any lattice dispersion.

8.1.1 Chain representation

For notational brevity, we concentrate on the general version of the single-orbital Anderson model. In this case, the Hilbert space of the local problem,

$$H_{\rm loc} = H_\mu + H_U, \tag{8.7}$$

$$H_\mu = -\mu(n_\uparrow + n_\downarrow), \tag{8.8}$$

$$H_U = U n_\uparrow n_\downarrow, \tag{8.9}$$

has dimension four. The discrete quantum number labeling the impurity states is the spin σ, $n_\sigma = d^\dagger_\sigma d_\sigma$ is the density operator for impurity electrons, and the chemical potential is $\mu = -\epsilon_d$. The bath and mixing terms are

$$H_{\rm bath} = \sum_{p\sigma} \varepsilon_p c^\dagger_{p\sigma} c_{p\sigma}, \tag{8.10}$$

$$H_{\rm mix} = \sum_{p\sigma} \left[V_{p\sigma} d^\dagger_\sigma c_{p\sigma} + V^*_{p\sigma} c^\dagger_{p\sigma} d_\sigma \right]. \tag{8.11}$$

https://doi.org/10.1017/CBO9780511902581.009 Published online by Cambridge University Press

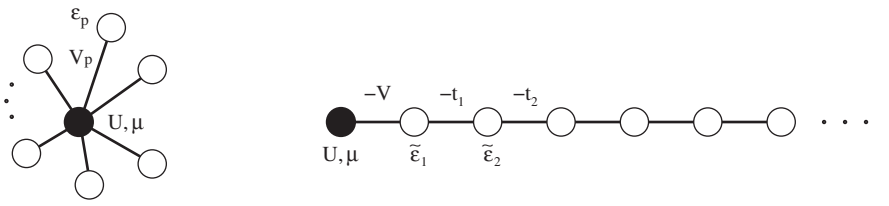

Figure 8.1 Left: Schematic representation of an Anderson impurity model. Spin up and down electrons on the impurity (black dot) interact with an on-site energy U and hop to a continuum of noninteracting bath levels with energy ε_p. The amplitudes for these transitions are given by the hybridization parameters V_p. Right: Chain representation of the Anderson impurity model. The hopping parameters V and t_i can be made positive by using a suitable gauge transformation (see Exercise 8.1).

An illustration of the Anderson impurity model is shown in the left-hand panel of Fig. 8.1.

This model can be mapped onto a semi-infinite chain whose first site is the impurity (right-hand panel of Fig. 8.1).[1] The mapping corresponds to a transformation of the operators $\{d, c_{p_1}, c_{p_2}, \ldots\}$ to new operators $\{d, c_1, c_2, \ldots\}$ such that $H_\mu + H_{\text{bath}} + H_{\text{mix}}$ becomes tridiagonal (Appendix J):

$$\begin{pmatrix} -\mu & V_{p_1} & V_{p_2} & V_{p_3} & \cdots \\ V_{p_1}^* & \varepsilon_{p_1} & & & \\ V_{p_2}^* & & \varepsilon_{p_2} & & \\ V_{p_3}^* & & & \varepsilon_{p_3} & \\ \vdots & & & & \ddots \end{pmatrix} \rightarrow \begin{pmatrix} -\mu & -V & & & \\ -V & \tilde{\varepsilon}_1 & -t_1 & & \\ & -t_1 & \tilde{\varepsilon}_2 & -t_2 & \\ & & -t_2 & \tilde{\varepsilon}_3 & \ddots \\ & & & \ddots & \ddots \end{pmatrix}.$$

In the chain representation, the impurity orbital is unchanged, and the hopping amplitude from the impurity to the first site of the chain is $V = (\sum_p |V_p|^2)^{1/2}$. We chose the phase factors in this transformation such that all hopping parameters are positive ($V \geq 0$, $t_i \geq 0$, $i = 1, 2, \ldots$). In Section 8.7, we use this fact to prove that continuous-time quantum Monte Carlo simulations of the Anderson impurity model do not have a sign problem.

8.1.2 Action formulation

As we did for the determinant methods, we formulate our impurity solvers in terms of imaginary-time Green's functions (or hybridization functions). Because of time-

[1] This representation was used by Wilson in his famous numerical renormalization group studies of the Anderson and Kondo impurity models (Wilson, 1975).

https://doi.org/10.1017/CBO9780511902581.009 Published online by Cambridge University Press

translation invariance, we can deconvolute the Dyson equation in imaginary time by using the Matsubara transformation

$$G(i\omega_n) = \int_0^\beta d\tau\, e^{i\omega_n \tau} G(\tau), \qquad G(\tau) = \frac{1}{\beta} \sum_n e^{-i\omega_n \tau} G(i\omega_n),$$

where the Matsubara frequencies are $\omega_n = (2n+1)\pi/\beta$ and $\beta = 1/T$ is the inverse temperature.

It is also useful to express the partition function and the imaginary-time Green's function in terms of the imaginary-time action. In Appendix K, we integrate out the bath degrees of freedom in the path-integral formalism and express the partition function of the Anderson impurity model as

$$Z = \mathrm{Tr}_d\left[\mathcal{T} e^{-S}\right],$$

with the action $S = S_{\mathrm{mix}} + S_{\mathrm{loc}}$ given by

$$S_{\mathrm{mix}} = \sum_\sigma \int_0^\beta d\tau d\tau' d_\sigma^\dagger(\tau') \Delta^\sigma(\tau' - \tau) d_\sigma(\tau), \tag{8.12}$$

$$S_{\mathrm{loc}} = \int_0^\beta d\tau \Big[-\mu(n_\uparrow(\tau) + n_\downarrow(\tau)) + U n_\uparrow(\tau) n_\downarrow(\tau) \Big]. \tag{8.13}$$

$\mathcal{T}$ is the time-ordering operator. The Green's function becomes[2]

$$G(\tau) = -\langle \mathcal{T} d(\tau) d^\dagger(0) \rangle_S = -\frac{1}{Z} \mathrm{Tr}_d\left[\mathcal{T} e^{-S} d(\tau) d^\dagger(0)\right].$$

The hybridization function $\Delta^\sigma(\tau' - \tau)$ in (8.12) represents the amplitude for hopping from the impurity into the bath at time τ and back onto the impurity at time τ'. It is a function of the bath energies and hybridization amplitudes and is most conveniently expressed in Matsubara frequency space:

$$\Delta^\sigma(i\omega_n) = \sum_p \frac{|V_{p\sigma}|^2}{i\omega_n - \varepsilon_p}. \tag{8.14}$$

It is also useful to introduce the Green's function of the noninteracting impurity,[3] $\mathcal{G}_0$, which is related to the hybridization function by

$$[\mathcal{G}_0^\sigma]^{-1}(i\omega_n) = i\omega_n + \mu - \Delta^\sigma(i\omega_n). \tag{8.15}$$

This function appears in the expression of the partition function in terms of Grassmann variables. We will use both $\mathcal{G}_0$ and Δ in the subsequent sections.

[2] This definition uses a sign convention different from the one used in the previous chapter.

[3] This function is sometimes called the "bath Green's function" (Georges et al., 1996). Since this name can be confusing, we avoid it in this book and instead use the term "Weiss Green's function."

https://doi.org/10.1017/CBO9780511902581.009 Published online by Cambridge University Press

8.2 Dynamical mean-field theory

Quantum impurity models are a key ingredient of the dynamical mean-field theory (DMFT), which provides an approximate description of correlated lattice models (Georges et al., 1996). The success of DMFT created a demand for more powerful and flexible impurity solvers and triggered the development of the continuous-time impurity solvers. We now briefly introduce the DMFT approximation, which maps an interacting lattice model, such as the Hubbard model, onto an effective impurity problem subject to a self-consistency condition for the bath.

8.2.1 Single-site effective model

To appreciate the basic strategy, we first recall the static mean-field approximation of the classical Ising model, illustrated in the left-hand panels of Fig. 8.2. There, we focus on one particular spin s_0 of the lattice and follow the venerable Weiss self-consistent molecular field prescription by replacing the remaining degrees of freedom by an effective external magnetic field $h_{\rm eff} = zmJ$, where z is the coordination number and m is the magnetization per site. The lattice system with interaction J between nearest-neighbor spins,

$$H^{\rm Ising} = -J \sum_{\langle ij \rangle} s_i s_j,$$

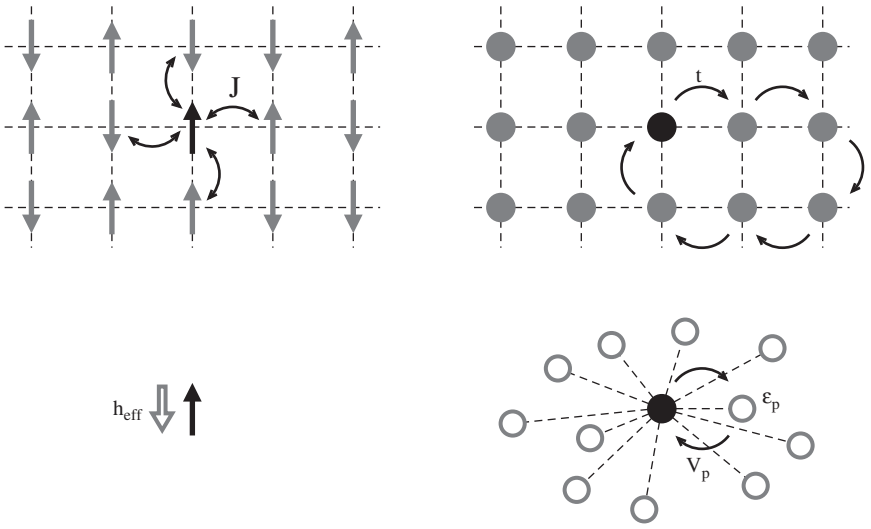

Figure 8.2 Left panels: Mapping of the classical Ising model to an effective single-site model (spin in an external magnetic field). Right panels: Mapping of the Hubbard model to an effective single-site model (one correlated site in an uncorrelated bath).

https://doi.org/10.1017/CBO9780511902581.009 Published online by Cambridge University Press

thus maps to the single-site effective model

$$H_{\text{eff}}^{\text{Ising}} = -h_{\text{eff}} s_0.$$

For this model, the magnetization is

$$m_{\text{eff}} = \tanh(\beta h_{\text{eff}}).$$

If we identify the magnetization m of the lattice problem with the magnetization m_{eff} of the single-site effective model, we obtain the self-consistency condition

$$m \equiv m_{\text{eff}} = \tanh(\beta z J m), \tag{8.16}$$

which implicitly determines the *mean field* h_{eff}. One can find the self-consistent solution by iteration.

We now turn to the Hubbard model and apply the same strategy. The model is

$$H_{\text{Hubbard}} = -t \sum_{\langle ij \rangle \sigma} (d_{i\sigma}^\dagger d_{j\sigma} + d_{j\sigma}^\dagger d_{i\sigma}) + U \sum_i n_{i\uparrow} n_{i\downarrow} - \mu \sum_{i\sigma} n_{i\sigma}$$

and describes electrons hopping between nearest neighbor sites of some lattice with amplitude t. Two electrons on the same site interact with energy U. We added a chemical potential term because we will work in the grand canonical ensemble. The noninteracting dispersion is obtained as the Fourier transform of the hopping matrix. For example, in the case of a one-dimensional lattice with lattice spacing a, $\epsilon_k = -2t \cos(ka)$.

Inspired by the Weiss molecular-field strategy, we focus on one particular site of the lattice (black dot in the right hand panels of Fig. 8.2) and replace the remaining degrees of freedom of the model by a bath of noninteracting levels and a hybridization term that connects the interacting site to the bath. The effective single-site problem thus becomes an Anderson impurity model,[4]

$$H_{\text{imp}} = \sum_{p\sigma} \varepsilon_p c_{p\sigma}^\dagger c_{p\sigma} + \sum_{p\sigma} (V_{p\sigma} d_\sigma^\dagger c_{p\sigma} + V_{p\sigma}^* c_{p\sigma}^\dagger d_\sigma) + U n_\uparrow n_\downarrow - \mu(n_\uparrow + n_\downarrow).$$

Here, the $d^\dagger$ create electrons on the impurity (black dot), $n_\sigma = d_\sigma^\dagger d_\sigma$, and the $c_p^\dagger$ create electrons in bath states (empty dots) labeled by a quantum number p. In this effective single-site model, hoppings from the impurity into the bath and back (bottom right panel of Fig. 8.2) represent processes in the original model where an electron hops from the black site into the lattice and returns to it after some excursion through the lattice (top right panel of Fig. 8.2). The hybridization parameters V_p give the amplitudes for such transitions.

[4] In the DMFT context, the bath energy levels ε_p of the impurity model are not directly related to the dispersion of the lattice model. We will denote the latter by ϵ_k. It is important to keep this distinction in notation in mind.

https://doi.org/10.1017/CBO9780511902581.009 Published online by Cambridge University Press

Our task now is to optimize the parameters ε_p and V_p such that the bath of the Anderson impurity model mimics the lattice environment as closely as possible. We do not yet know ε_p and V_p. They are the analogs of h_{eff} and thus are the parameters we need to adjust self-consistently. If we work with the impurity action, the bath properties are encoded in $\Delta(\tau)$ or $\mathcal{G}_0(\tau)$, and these functions thus play the role of the mean field. It is a *dynamical* mean field, because the hybridization function or Weiss Green's function depends on (imaginary) time or frequency.

The self-consistent solution is constructed in such a way that the impurity Green's function $G_{\text{imp}}(i\omega_n)$ reproduces the *local* lattice Green's function $G_{\text{loc}}(i\omega_n) \equiv G_{i,i}(i\omega_n)$. In other words, if $G(k, i\omega_n)$ is the momentum-dependent lattice Green's function of the Hubbard model, we seek bath parameters and hybridizations such that[5]

$$\int (dk) G(k, i\omega_n) \equiv G_{\text{imp}}(i\omega_n). \tag{8.17}$$

8.2.2 DMFT approximation

We obtain the solution of (8.17) iteratively. However, in contrast to the Ising case (8.16), it is not immediately clear how we can use the self-consistency condition (8.17) to update the dynamical mean field. To define a practical procedure, we have to relate the left-hand side of (8.17) to impurity model quantities. This step involves, as the essential approximation of the DMFT method, a significant simplification of the momentum-dependence of the lattice self-energy.

The self-energy describes the effect of interactions on the propagation of electrons. In the noninteracting model, the lattice Green's function is $G_0(k, i\omega_n) = [i\omega_n + \mu - \epsilon_k]^{-1}$, with ϵ_k being the Fourier transform of the hopping matrix. The Green's function of the interacting model is $G(k, i\omega_n) = [i\omega_n + \mu - \epsilon_k - \Sigma(k, i\omega_n)]^{-1}$ with $\Sigma(k, i\omega_n)$ the lattice self-energy. Therefore

$$\Sigma(k, i\omega_n) = G_0^{-1}(k, i\omega_n) - G^{-1}(k, i\omega_n).$$

Similarly, we obtain the impurity self-energy

$$\Sigma_{\text{imp}}(i\omega_n) = \mathcal{G}_0^{-1}(i\omega_n) - G_{\text{imp}}^{-1}(i\omega_n),$$

with $\mathcal{G}_0^{-1}$ defined in (8.15). The DMFT approximation is the identification of the lattice self-energy with the momentum-independent impurity self-energy,

$$\Sigma(k, i\omega_n) \approx \Sigma_{\text{imp}}(i\omega_n).$$

This approximation allows us to rewrite the self-consistency equation (8.17) as

[5] $\int (dk)$ denotes a normalized integral over the Brillouin zone.

https://doi.org/10.1017/CBO9780511902581.009 Published online by Cambridge University Press

$$\int (dk)[i\omega_n + \mu - \epsilon_k - \Sigma_{\rm imp}(i\omega_n)]^{-1} \equiv G_{\rm imp}(i\omega_n). \tag{8.18}$$

Since both $G_{\rm imp}(i\omega_n)$ and $\Sigma_{\rm imp}(i\omega_n)$ are determined by the impurity model parameters ε_p and V_p (or the function $\Delta(\tau)$ or $\mathcal{G}_0(\tau)$), (8.18) defines a self-consistency condition for these parameters (or functions).

8.2.3 DMFT self-consistency loop

We now formulate the self-consistency loop for the Weiss Green's function $\mathcal{G}_0(i\omega_n)$. Starting from an arbitrary initial $\mathcal{G}_0(i\omega_n)$ (e.g., the local Green's function of the noninteracting lattice model), we iterate the following steps until convergence (Algorithm 26):

1. Solve the impurity problem, that is, compute the impurity Green's function $G_{\rm imp}(i\omega_n)$ for the given $\mathcal{G}_0(i\omega_n)$.
2. Extract the self-energy of the impurity model: $\Sigma_{\rm imp}(i\omega_n) = \mathcal{G}_0^{-1}(i\omega_n) - G_{\rm imp}^{-1}(i\omega_n)$.
3. Identify the lattice self-energy with the impurity self-energy, $\Sigma(k, i\omega_n) = \Sigma_{\rm imp}(i\omega_n)$ (DMFT approximation), and compute the local lattice Green's function $G_{\rm loc}(i\omega_n) = \int (dk)[i\omega_n + \mu - \epsilon_k - \Sigma_{\rm imp}(i\omega_n)]^{-1}$.
4. Apply the DMFT self-consistency condition, $G_{\rm loc}(i\omega_n) = G_{\rm imp}(i\omega_n)$, and use it to define a new Weiss Green's function $\mathcal{G}_0^{-1}(i\omega_n) = G_{\rm loc}^{-1}(i\omega_n) + \Sigma_{\rm imp}(i\omega_n)$.

The computationally expensive step is the solution of the impurity problem (step 1). When the loop converges, the bath contains information about the topology of the lattice (through the density of states) and about the phase (metal, Mott insulator, antiferromagnetic insulator, etc.). The impurity, which exchanges

Algorithm 26 DMFT self-consistency loop. (Using Eq. (8.15), the loop can also be formulated in terms of the hybridization function Δ, instead of the Weiss Green's function $\mathcal{G}_0$.)

Input: Some initial guess for the Weiss Green's function $\mathcal{G}_0(i\omega_n)$, noninteracting dispersion ϵ_k, chemical potential μ, inverse temperature β.

repeat

Compute $G_{\rm imp}(i\omega_n)$ for given $\mathcal{G}_0(i\omega_n)$; ▷ Solve impurity problem

$\Sigma_{\rm imp}(i\omega_n) = \mathcal{G}_0^{-1}(i\omega_n) - G_{\rm imp}^{-1}(i\omega_n)$;

$G_{\rm loc}(i\omega_n) = \int (dk)[i\omega_n + \mu - \epsilon_k - \Sigma_{\rm imp}(i\omega_n)]^{-1}$;

$\mathcal{G}_0^{-1}(i\omega_n) \leftarrow G_{\rm loc}^{-1}(i\omega_n) + \Sigma_{\rm imp}(i\omega_n)$;

until $G_{\rm loc}$ is converged.

return $G_{\rm loc}$.

https://doi.org/10.1017/CBO9780511902581.009 Published online by Cambridge University Press

electrons with the bath, thus behaves, at least to some extent, as if it were a site of the lattice.

Obviously, a single-site impurity model does not capture all the physics. In particular, the DMFT approximation neglects all spatial fluctuations. These fluctuations are important, for example, in low-dimensional systems. The DMFT formalism is believed to provide a qualitatively correct description of three-dimensional unfrustrated lattice models. It becomes exact in the limit of infinite dimension (Metzner and Vollhardt, 1989) or infinite coordination number (where spatial fluctuations are negligible), in the noninteracting limit ($U = 0$ implies $\Sigma = 0$), and in the atomic limit ($t = 0$ implies $\Delta = 0$).

8.2.4 Simulation of strongly correlated materials

The DMFT formalism describes band-like behavior (renormalized quasi-particle bands) *and* atomic-like behavior (Hubbard bands). It captures the competition between electron localization and delocalization, which plays a crucial role in the physics of strongly correlated materials. One possible approach to simulate real compounds is to combine the DMFT formalism with electronic structure calculations in the local density approximation (LDA). The resulting formalism is called "LDA+DMFT" (Kotliar et al., 2006).

The idea is to use the Kohn-Sham eigenvalues $\epsilon^{\mathrm{KS}}_{n,k}$, obtained from an LDA calculation, in the self-consistency equation (8.18). To describe the strong correlation effects experienced by the d-electrons (e.g., in a transition metal oxide) or the f-electrons (e.g., in an actinide), we add a frequency-dependent, but local self-energy to the corresponding orbitals. This self-energy is obtained from a self-consistently defined impurity problem.

An important issue in practical implementations of the LDA+DMFT scheme is the choice of orbitals. The LDA calculation yields the extended Kohn-Sham wave functions $\psi_{n,k}$. The impurity model, on the other hand, describes the interactions between electrons that occupy localized, atomic-like orbitals. One common choice of orbitals is a Wannier basis, for example, the *maximally localized Wannier orbitals* (Marzari and Vanderbilt, 1997) that minimize the expectation value of the operator r^2. In this basis $\{\phi_l\}$, we identify the subset $\{\phi_\alpha\}$ of "strongly correlated" orbitals with d- or f-character and then define an interaction term

$$H_U = \frac{1}{2} \sum_{i\alpha\beta\gamma\delta} U^{\alpha\beta\gamma\delta} d^\dagger_{i\alpha} d^\dagger_{i\beta} d_{i\gamma} d_{i\delta}.$$

The interaction parameters $U^{\alpha\beta\gamma\delta}$ are either treated as adjustable parameters or extracted from the LDA band structure using techniques called "constrained LDA"

https://doi.org/10.1017/CBO9780511902581.009 Published online by Cambridge University Press

or "constrained RPA."[6] Let us emphasize that the interaction parameters depend on the choice of orbitals. More localized orbitals result in larger interaction terms. In a Wannier-orbital basis, this also means that the number of (strongly and weakly correlated) bands kept in the simulation affects the interaction parameters, because a larger number of bands implies more localized and atomic-like orbitals.

The Kohn-Sham Hamiltonian

$$H^{\mathrm{KS}} = \sum_{klm} (h_k^{\mathrm{KS}})_{lm} d_{kl}^\dagger d_{km},$$

which is diagonal in the band basis, becomes a nontrivial matrix in the localized orbital basis $\{\phi_l\}$. Explicitly, $h_k^{\mathrm{KS}} = O_k \epsilon_k^{\mathrm{KS}} O_k^{-1}$, where O_k is the matrix describing the basis transformation from $\{\psi_{n,k}\}$ to $\{\phi_l\}$. By combining H^{KS}, the local interaction term H_U, and a "double counting term"

$$H_{DC} = -\sum_{i\alpha} e_{DC}^{\alpha} d_{i\alpha}^\dagger d_{i\alpha},$$

we obtain the model to be solved within the DMFT approximation:

$$H = H^{\mathrm{KS}} + H_U + H_{DC}. \tag{8.19}$$

We need the double counting correction for the following reason: While density functional theory (on which the LDA approximation is based) does not take into account all electronic correlation effects, it does capture some of them. If we then explicitly describe the local interactions in the strongly correlated orbitals via the H_U-term, some interaction contributions appear twice. The double counting term is supposed to compensate for this by shifting the correlated orbitals by e_{DC}.

Currently, there is no clean and consistent solution to the double counting problem. The exchange-and-correlation potential, which describes the correlation effects within density functional theory, is (within the LDA) a *nonlinear* functional

[6] In the *constrained LDA* technique (Anisimov and Gunnarsson, 1991), we calculate the interaction as the derivative of the energy with respect to the charge. This approach requires different LDA calculations, in which the charges in the orbitals are fixed at different values. In the *constrained RPA* technique (Aryasetiawan et al., 2004), on the other hand, we compute polarization functions using the random phase approximation (RPA), that is, by summing bubble diagrams made of LDA propagators. The total polarization P is split into the polarization P_d associated with transitions between "strongly correlated" bands, and the remaining polarization $P_r = P - P_d$. We then define a *partially screened* interaction W_r, which has the property that if it is screened further by the polarization P_d, it gives the fully screened interaction $W = v/(1 - Pv)$ (v here is the bare Coulomb interaction): $W = W_r/(1 - P_d W_r)$. One finds that $W_r = v/(1 - P_r v)$. The interaction parameters $U^{\alpha\beta\gamma\delta}$ are then defined as the matrix elements of W_r in the localized basis $\{\phi_\alpha\}$. We note that the polarizations are *frequency dependent*, and thus the interaction parameters $U^{\alpha\beta\gamma\delta}$ are also frequency dependent. This result makes physical sense: At high frequencies (above the plasmon frequency in a metal) screening is not effective, and the interaction is essentially the bare Coulomb interaction v (typically about 20 eV in transition metal compounds), while slow charge fluctuations are screened by the surrounding electrons, resulting in a static interaction of typically only a few eV.

of the *total* density, so we cannot determine the contribution of the d- or f-electrons to the exchange-and-correlation energy. In practice, we invoke double counting terms such as $e^{\alpha}_{DC} = \langle U \rangle (\langle n_{\text{corr}} \rangle - \frac{1}{2})$,[7] with $\langle U \rangle$ being the average of the interaction parameters and $\langle n_{\text{corr}} \rangle$ being the average occupancy of the correlated orbitals. Such an orbital-independent shift preserves the crystal-field splittings in the LDA band structure.

Finally, we add a chemical potential term and adjust the chemical potential μ to obtain the correct total number of electrons in the correlated and uncorrelated orbitals.

To compute the (local) self-energy within the DMFT approximation, we solve an impurity model with interaction terms identical to those in H_U. This solution yields the matrices $[G_{\text{imp}}]_{\alpha\beta}$ and $[\Sigma_{\text{imp}}]_{\alpha\beta}$, which are defined in the subspace of correlated orbitals. To write the self-consistency condition, we define the matrix Σ in the full space of localized orbitals $\{\phi_l\}$:

$$\Sigma(i\omega_n) = \left(\begin{array}{c|c} \Sigma_{\text{imp}}(i\omega_n) & 0 \\ \hline 0 & 0 \end{array} \right), \tag{8.20}$$

where the first diagonal block corresponds to the strongly correlated orbitals (five, in the case of a full d-shell) and the second diagonal block to the weakly correlated ones. Similarly, the double counting term is a (diagonal) matrix acting on the full space:

$$E_{DC} = \left(\begin{array}{c|c} -e_{DC} & 0 \\ \hline 0 & 0 \end{array} \right). \tag{8.21}$$

The self-consistency condition, which fixes the dynamical mean field $\mathcal{G}_0$ or Δ, becomes

$$\left[\int (dk) \left[(i\omega_n + \mu) I - h^{\text{KS}}_k - \Sigma(i\omega_n) - E_{DC} \right]^{-1} \right]_{\alpha\beta} \equiv [G_{\text{imp}}(i\omega_n)]_{\alpha\beta}. \tag{8.22}$$

Note that while the self-consistency condition involves only the correlated block of the local lattice Green's function, the weakly correlated orbitals enter the calculation through the matrix inversion. We summarize the computational scheme for the LDA+DMFT calculation in Algorithm 27.

[7] This double counting prescription follows from a mean-field estimate for the interaction energy: $E_{\text{corr}} \approx \frac{1}{2} \langle U \rangle \langle n_{\text{corr}} \rangle (\langle n_{\text{corr}} \rangle - 1)$. For a more detailed discussion of the double counting issue, see Anisimov et al. (1991); Aichhorn et al. (2011); Haule (2015).

https://doi.org/10.1017/CBO9780511902581.009 Published online by Cambridge University Press

Algorithm 27 LDA+DMFT self-consistency loop.

Input: Some ($N_{\rm corr} \times N_{\rm corr}$) Weiss Green's function matrix $\mathcal{G}_0(i\omega_n)$, Kohn-Sham Hamiltonian $h_k^{\rm KS}$ in a localized basis ($N_{\rm tot} \times N_{\rm tot}$), total number of electrons $n_{\rm tot}^{\rm target}$, some initial guess for the chemical potential μ, inverse temperature β.

repeat

  repeat

    Compute $G_{\rm imp}(i\omega_n)$ for given $\mathcal{G}_0(i\omega_n)$; ▷ Solve impurity problem

    $\Sigma_{\rm imp}(i\omega_n) = \mathcal{G}_0^{-1}(i\omega_n) - G_{\rm imp}^{-1}(i\omega_n)$;

    Define the $N_{\rm tot} \times N_{\rm tot}$ matrices Σ (8.20) and E_{DC} (8.21) ;

    $G_{\rm loc}(i\omega_n) = \int (dk)[(i\omega_n + \mu)I - h_k^{\rm KS} - \Sigma(i\omega_n) - E_{DC}]^{-1}$;

    Extract $N_{\rm corr} \times N_{\rm corr}$ correlated block $G_{\rm loc}^{\rm corr}(i\omega_n)$ from $G_{\rm loc}(i\omega_n)$;

    $\mathcal{G}_0^{-1}(i\omega_n) \leftarrow (G_{\rm loc}^{\rm corr}(i\omega_n))^{-1} + \Sigma_{\rm imp}(i\omega_n)$;

  until $G_{\rm loc}$ is converged.

  Compute $n_{\rm tot} = -\sum_{i=1}^{N_{\rm tot}} [G_{\rm loc}(\beta_-)]_{ii}$;

  if $n_{\rm tot} < n_{\rm tot}^{\rm target}$ **then**

    Increase μ ;

  else

    Decrease μ ;

  end if

until $n_{\rm tot}$ is converged.

return $G_{\rm loc}$.

8.2.5 Cluster extensions

To capture the effect of short-range spatial fluctuations, cluster extensions of dynamical mean field theory were developed (Maier et al., 2005). In these extensions, a cluster of several sites, instead of a single site, is embedded in a self-consistently determined bath. This embedding allows us to describe the short-range spatial correlations on the cluster explicitly, while treating the longer range correlations on a mean-field level. This approach is the analog of the Bethe-Peierls cluster molecular-field approximation (Bethe, 1935), which extended the Weiss molecular field theory for classical spin models from a single site to a cluster of sites to capture short-range spin correlations.

In a cluster DMFT, we divide the lattice into a superlattice of clusters containing n_c sites and apply the DMFT procedure to the superlattice (Lichtenstein and Katsnelson, 2000). The cluster Green's functions and self-energies are now matrices of size $n_c \times n_c$, while ϵ_k becomes a matrix $\hat{t}(k)$, defined as the Fourier transform of the hopping matrix on the superlattice. The momenta k are those of the reduced Brillouin zone of the superlattice.

https://doi.org/10.1017/CBO9780511902581.009 Published online by Cambridge University Press

Figure 8.3 Decomposition of the one-dimensional Hubbard chain into two-site clusters (dashed boxes).

To be more specific, let us consider a one-dimensional Hubbard chain, with lattice spacing a, that we decompose into two-site clusters (Fig. 8.3). The hopping matrix then has the form

$$\left(\begin{array}{c|cc|cc|c} \ddots & -t & & & & \\ \hline -t & 0 & -t & & & \\ & -t & 0 & -t & & \\ \hline & & -t & 0 & -t & \\ & & & -t & 0 & -t \\ \hline & & & & -t & \ddots \end{array}\right),$$

which after Fourier transformation on the superlattice with spacing $2a$ becomes

$$\begin{aligned} -\hat{t}(k) &= e^{ik0}\begin{pmatrix} 0 & t \\ t & 0 \end{pmatrix} + e^{ik(2a)}\begin{pmatrix} 0 & 0 \\ t & 0 \end{pmatrix} + e^{ik(-2a)}\begin{pmatrix} 0 & t \\ 0 & 0 \end{pmatrix} \\ &= \begin{pmatrix} 0 & t(1+e^{-i2ka}) \\ t(1+e^{i2ka}) & 0 \end{pmatrix}. \end{aligned} \tag{8.23}$$

The self-consistency condition, which fixes the 2×2 matrix of the dynamical mean field $\mathcal{G}_0$ or Δ, is now

$$\int_{\text{reduced BZ}} (dk)[(i\omega_n + \mu)\hat{I} - \hat{t}(k) - \hat{\Sigma}_{\text{imp}}(i\omega_n)]^{-1} = \hat{G}_{\text{imp}},$$

with the reduced Brillouin zone $-\pi/2a \le k < \pi/2a$.

As is evident from the hopping matrix (8.23), the cluster DMFT formalism breaks translational invariance within the cluster. There is an alternative cluster DMFT, called the *dynamical cluster approximation* (DCA), which enforces this symmetry (Hettler et al., 1998). The two-site DCA corresponds to the hopping matrix

$$-\hat{t}_{\text{DCA}}(k) = \begin{pmatrix} 0 & 2t\cos(ka) \\ 2t\cos(ka) & 0 \end{pmatrix}. \tag{8.24}$$

In the "momentum basis," $\{d_{K=0} = \frac{1}{\sqrt{2}}(d_1 + d_2), d_{K=\frac{\pi}{a}} = \frac{1}{\sqrt{2}}(d_1 - d_2)\}$, the Green's functions and self-energies are diagonal matrices, and the self-consistency condition for each "momentum sector" K is

$$\int_{\text{sector } K} (dk)[i\omega_n + \mu - \epsilon_k - \Sigma^K_{\text{imp}}(i\omega_n)]^{-1} = G^K_{\text{imp}}, \tag{8.25}$$

https://doi.org/10.1017/CBO9780511902581.009 Published online by Cambridge University Press

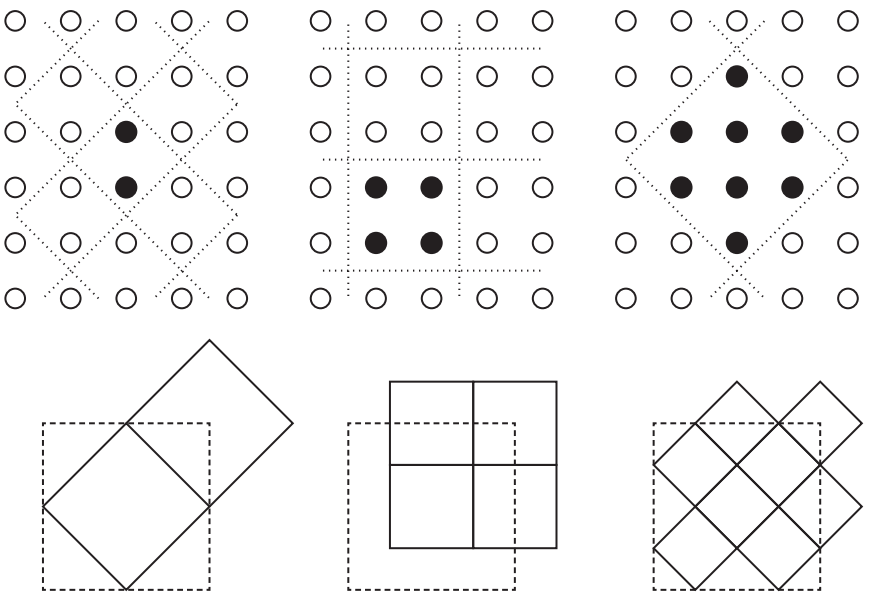

Figure 8.4 Two-, four-, and eight-site DCA approximation for the two-dimensional Hubbard model. The top panels show the (periodized) real-space clusters, and the bottom panels illustrate the corresponding decompositions of the first Brillouin zone (dashed square) into equal-sized sectors.

with $\epsilon_k = -2t\cos(ka)$. In our two-site example, sector $K = 0$ corresponds to $-\pi/2a \leq k < \pi/2a$, while sector $K = \pi/a$ corresponds to $\pi/2a \leq k < 3\pi/2a$. The first Brillouin zone thus decomposes into two sectors of equal size, centered at the reciprocal lattice vectors of the periodized two-site cluster. Figure 8.4 illustrates how the DCA concept extends to the two-dimensional square lattice. The top panels show the (periodized) real-space clusters with two, four, and eight sites and the bottom panels the corresponding tiling of the first Brillouin zone.[8]

The periodized real-space clusters of the DCA impurity model involve renormalized hoppings, which can be obtained as the Fourier transform of the patch-averaged dispersion (see Exercise 8.8).

8.3 General strategy

Quantum impurity models are (0+1)-dimensional quantum field theories and as such are computationally much more tractable than interacting lattice models. Our objective is computing the impurity Green's function[9]

[8] In DCA, the matrix $[\mathcal{G}_0]_{ij}$ connects all pairs of sites, and it is translation invariant within the cluster. The equivalent pairs of sites can be identified by considering the superlattice of clusters, indicated by the dotted lines in Fig. 8.4.

[9] The sign convention here differs from the one used in the previous chapter.

https://doi.org/10.1017/CBO9780511902581.009 Published online by Cambridge University Press

$$G(\tau) = -\langle \mathcal{T} d(\tau) d^\dagger(0) \rangle = -\frac{1}{Z} \mathrm{Tr}\Big[e^{-(\beta-\tau)H} d e^{-\tau H} d^\dagger \Big], \tag{8.26}$$

where $Z = \mathrm{Tr}[e^{-\beta H}]$ is the impurity model partition function, β is the inverse temperature, $\mathcal{T}$ is the (imaginary) time-ordering operator, and $\mathrm{Tr} = \mathrm{Tr}_d \mathrm{Tr}_c$ is the trace over the impurity and bath states. In the last expression we assumed that $0 \le \tau < \beta$.

Continuous-time Monte Carlo algorithms expand the partition function into a series of "diagrams" and stochastically sample these diagrams (Gull et al., 2011). Following the general procedure outlined in Chapter 2, we represent the partition function as a sum (or more precisely as an integral) over configurations C with weight w_C,

$$Z = \sum_C w_C, \tag{8.27}$$

and implement a random walk $C_1 \to C_2 \to C_3 \to \cdots$ in configuration space in such a way that ergodicity and detailed balance are satisfied. Using sign-weighted averages (Section 5.4), we estimate the impurity Green's function from a finite number M of measurements as

$$G = \sum_C \frac{w_C G_C}{Z} = \frac{\sum_C |w_C| \mathrm{sign}_C G_C}{\sum_C |w_C| \mathrm{sign}_C} \approx \frac{\sum_{i=1}^M \mathrm{sign}_{C_i} G_{C_i}}{\sum_{i=1}^M \mathrm{sign}_{C_i}} \equiv \frac{\langle \mathrm{sign} \cdot G \rangle_{\mathrm{MC}}}{\langle \mathrm{sign} \rangle_{\mathrm{MC}}}. \tag{8.28}$$

Our first step toward detailing the continuous-time solvers is to express the partition function as an imaginary-time-ordered exponential in an *interaction representation*. To do this, we split the Hamiltonian into two parts, $H = H_1 + H_2$, and define the imaginary-time-dependent operators in the interaction representation as $O(\tau) = e^{\tau H_1} O e^{-\tau H_1}$. In this representation, the partition function becomes $Z = \mathrm{Tr}\Big[e^{-\beta H_1} \mathcal{T} e^{-\int_0^\beta d\tau H_2(\tau)} \Big]$.[10]

Next, we expand the time-ordered exponential into a power series,

$$Z = \sum_{n=0}^{\infty} \int_0^\beta d\tau_1 \cdots \int_{\tau_{n-1}}^\beta d\tau_n \mathrm{Tr}\Big[e^{-(\beta-\tau_n)H_1} (-H_2) \cdots e^{-(\tau_2-\tau_1)H_1} (-H_2) e^{-\tau_1 H_1} \Big]. \tag{8.29}$$

We now have a representation of the partition function of the form (8.27), namely, as an infinite sum over the weights of certain configurations. The configurations are collections of time points on the imaginary-time interval: $C = \{\tau_1, \ldots, \tau_n\}$, $n = 0, 1, \ldots$, where we assume the imaginary-time ordering $\tau_i < \tau_{i+1}$ and the restriction $\tau_i \in [0, \beta)$. In contrast to the sampling we discussed in

[10] We can understand this formula by defining the operator $A(\beta) = e^{\beta H_1} e^{-\beta H}$ and writing the partition function as $Z = \mathrm{Tr}[e^{-\beta H_1} A(\beta)]$. The operator $A(\beta)$ satisfies $dA/d\beta = e^{\beta H_1}(H_1 - H) e^{-\beta H} = -H_2(\beta) A(\beta)$, the solution of which is $A(\beta) = \mathcal{T} \exp\big[-\int_0^\beta d\tau H_2(\tau) \big]$.

https://doi.org/10.1017/CBO9780511902581.009 Published online by Cambridge University Press

Chapter 7, where each configuration had a fixed number of local variables, here the number of time points in a configuration varies, reflecting the sampling of different orders in the power series. The expression for the Monte Carlo weights is

$$w_C = \mathrm{Tr}\Big[e^{-(\beta-\tau_n)H_1}(-H_2)\cdots e^{-(\tau_2-\tau_1)H_1}(-H_2)e^{-\tau_1 H_1}\Big](d\tau)^n. \tag{8.30}$$

There are two complementary continuous-time Monte Carlo techniques: (i) the *weak-coupling approach*, which scales favorably with system size (that is, the number of correlated sites or orbitals in the impurity model) and allows the efficient simulation of relatively large impurity clusters with simple interactions, and (ii) the *strong-coupling approach*, which can handle impurity models with strong interactions among multiple orbitals. For simplicity, we continue to focus on the single-orbital Anderson impurity model defined in (8.8)–(8.11). In this case, the weak-coupling continuous-time Monte Carlo approach expands Z in powers of the interaction U in an interaction representation where the imaginary-time evolution is determined by the *quadratic* part $H_\mu + H_{\mathrm{bath}} + H_{\mathrm{mix}}$ of the Hamiltonian. The complementary strong-coupling approach expands Z in powers of the impurity-bath hybridization term H_{mix} in an interaction representation where the imaginary-time evolution is determined by the *local* part $H_\mu + H_U + H_{\mathrm{bath}}$ of the Hamiltonian. The details of how we sample the weights (8.30) and how we measure observables depend on which continuous-time approach we are using.

8.4 Weak-coupling approach

The weak-coupling continuous-time impurity solver (Rubtsov et al., 2005) expands the partition function in powers of $H_2 = H_U$.[11] Equation (8.30) then gives the weight of a configuration of *n interaction vertices*. Since $H_1 = H - H_2 = H_\mu + H_{\mathrm{bath}} + H_{\mathrm{mix}}$ is quadratic, we use Wick's theorem to evaluate the trace. The result is a product of two determinants of $n \times n$ matrices (one for each electron spin). The elements of these matrices are the Weiss Green's functions $\mathcal{G}_0^\sigma$ for the time intervals defined by the vertex positions:

$$\begin{aligned}\frac{w_C}{Z_0} &= (-Ud\tau)^n \frac{1}{Z_0}\mathrm{Tr}\Big[e^{-(\beta-\tau_n)H_1}n_\uparrow n_\downarrow \cdots e^{-(\tau_2-\tau_1)H_1}n_\uparrow n_\downarrow e^{-\tau_1 H_1}\Big] \\ &= (-Ud\tau)^n \prod_\sigma \det M_\sigma^{-1},\end{aligned}$$

where

$$[M_\sigma^{-1}]_{ij} = \mathcal{G}_0^\sigma(\tau_i - \tau_j),$$

[11] A related algorithm, based on an expansion in powers of $H_U - K/\beta$ (with K some nonzero constant), is the *continuous-time auxiliary field method* discussed in Appendix L.

https://doi.org/10.1017/CBO9780511902581.009 Published online by Cambridge University Press

$\mathcal{G}_0^\sigma(\tau) = -\mathrm{Tr}[e^{-\beta H_1}\mathcal{T}d(\tau)d^\dagger(0)]/Z_0$, and $Z_0 = \mathrm{Tr}[e^{-\beta H_1}]$ is the partition function of the noninteracting model.[12] For the diagonal elements, we adopt the convention $[M_\sigma^{-1}]_{ii} = \mathcal{G}_0^\sigma(0^-)$.

At this point, we notice a potential sign problem. In the paramagnetic phase, where $\mathcal{G}_0^\uparrow = \mathcal{G}_0^\downarrow$, the product of determinants is positive, which means that for a repulsive interaction ($U > 0$) odd perturbation orders yield negative weights. Except in the particle-hole symmetric case, where odd perturbation orders vanish, these odd order configurations ostensibly cause a sign problem. Fortunately, we can solve this sign problem by shifting the chemical potentials for up- and down-spins in an appropriate way. To do so, we rewrite the interaction term as (Assaad and Lang, 2007)

$$H_U = \frac{U}{2}\sum_s \prod_\sigma (n_\sigma - \alpha_\sigma(s)) + \frac{U}{2}(n_\uparrow + n_\downarrow) + U\left[\left(\frac{1}{2}+\delta\right)^2 - \frac{1}{4}\right], \tag{8.31}$$

with

$$\alpha_\sigma(s) = \frac{1}{2} + \sigma s\left(\frac{1}{2}+\delta\right). \tag{8.32}$$

Here, δ is some constant and $s = \pm 1$ is an auxiliary Ising variable. This construction is not a Hubbard-Stratonovich transformation, but simply a shift in the zero of energy. The constant $U[(\frac{1}{2}+\delta)^2 - \frac{1}{4}]$ in (8.31) is irrelevant and will be ignored in the following. We absorb the contribution $\frac{1}{2}U(n_\uparrow + n_\downarrow)$ into the noninteracting Green's function by shifting the chemical potential as $\mu \to \mu - \frac{1}{2}U$. Explicitly, we redefine the Weiss Green's function as[13]

$$[\mathcal{G}_0^\sigma]^{-1} = i\omega_n + \mu - \Delta^\sigma \to [\tilde{\mathcal{G}}_0^\sigma]^{-1} = i\omega_n + \mu - \tfrac{1}{2}U - \Delta^\sigma.$$

The introduction of an Ising variable s_i at each vertex position τ_i enlarges the configuration space exponentially. A configuration C now corresponds to a collection of auxiliary spin variables defined on the imaginary-time interval: $C = \{(\tau_1, s_1), (\tau_2, s_2), \ldots, (\tau_n, s_n)\}$. The probability of these configurations is

$$w_C = \tilde{Z}_0(-Ud\tau/2)^n \prod_\sigma \det \tilde{M}_\sigma^{-1}, \tag{8.33}$$

where

$$[\tilde{M}_\sigma^{-1}]_{ij} = \tilde{\mathcal{G}}_0^\sigma(\tau_i - \tau_j) - \alpha_\sigma(s_i)\delta_{ij}. \tag{8.34}$$

[12] We note that in the DMFT framework discussed in Section 8.2.3, the function $\mathcal{G}_0^\sigma$ is determined directly by the self-consistency loop, without reference to a Hamiltonian. For the purpose of the present discussion, we may, however, assume that we know H_{bath} and H_{mix} terms whose parameters yield $\mathcal{G}_0^\sigma$ through (8.14) and (8.15).

[13] In a DMFT calculation, this means that the shifted chemical potential is used within the self-consistency loop.

https://doi.org/10.1017/CBO9780511902581.009 Published online by Cambridge University Press

In Section 8.7 we show that for $\delta \geq 0$ all Monte Carlo configurations for the Anderson impurity model have positive weights.

8.4.1 Sampling

For ergodicity it is sufficient that the sampling inserts the auxiliary spins with random orientation at random times and removes randomly chosen spins. By adopting the Metropolis-Hastings algorithm (Section 2.5.2) to generate the random walk in configuration space, we have an acceptance matrix

$$A(C' \leftarrow C) = \min[1, \mathcal{R}(C' \leftarrow C)],$$

where

$$\mathcal{R}(C' \leftarrow C) = \frac{w(C')T(C \leftarrow C')}{w(C)T(C' \leftarrow C)}$$

and $T(C' \leftarrow C)$ denotes the proposal probability for the move from C to C'. We use (8.33) to compute the ratio of the weights. To complete the description of the sampling we need to specify proposal probabilities for the insertion and removal of an auxiliary spin. There is some flexibility in choosing them. We illustrate reasonable choices in Fig. 8.5. For the insertion, we pick a random time in $[0, \beta)$ and a random orientation for the new spin, while for the removal, we simply pick a random spin. The corresponding proposal probabilities are

$$T(n+1 \leftarrow n) = \tfrac{1}{2}(d\tau/\beta), \quad T(n \leftarrow n+1) = 1/(n+1). \tag{8.35}$$

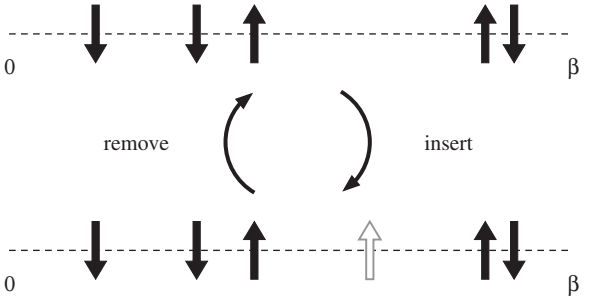

Figure 8.5 Local update in the weak-coupling method. The dashed line represents the imaginary-time interval $[0, \beta)$. We increase the perturbation order by adding an auxiliary spin with random orientation at a random time and decrease it by removing a randomly chosen auxiliary spin.

https://doi.org/10.1017/CBO9780511902581.009 Published online by Cambridge University Press

The first step is choosing with equal probability whether we insert or remove. If we insert, then we are going from a configuration with n spins to a configuration with $n+1$ spins, and from (8.33) and the above choices for T, the acceptance matrix becomes $A(n+1 \leftarrow n) = \min[1, \mathcal{R}_{\text{insert}}(n+1 \leftarrow n)]$ with

$$\mathcal{R}_{\text{insert}}(n+1 \leftarrow n) = \frac{-\beta U}{n+1} \prod_{\sigma} \frac{\det[\tilde{M}_{\sigma}^{(n+1)}]^{-1}}{\det[\tilde{M}_{\sigma}^{(n)}]^{-1}}. \tag{8.36}$$

The acceptance probability for the removal follows from

$$\mathcal{R}_{\text{remove}}(n \leftarrow n+1) = 1/\mathcal{R}_{\text{insert}}(n+1 \leftarrow n). \tag{8.37}$$

8.4.2 Determinant ratios and fast matrix updates

From (8.36), we see that each update requires the calculation of a ratio of two determinants. We encountered a similar problem in the determinant method: Computing the determinant of a matrix of size $n \times n$ is an $O(n^3)$ operation. However, each insertion or removal of a vertex (or spin) merely changes one row and one column of the matrix M_{σ}^{-1} (or $\tilde{M}_{\sigma}^{-1}$).[14] As in the case of the determinant method, we use a result from linear algebra to evaluate this ratio in a time $O(n^2)$ for insertion and $O(1)$ for removal. The trick here differs only slightly from the one used in the determinant method.

To explain it, we first note that the objects we store and manipulate, besides the lists of the times $\{\tau_i\}$ (or times and spins $\{(\tau_i, s_i)\}$), are the matrices $M_{\sigma} = [\mathcal{G}_0^{\sigma}]^{-1}$, not $M_{\sigma}^{-1} = [\mathcal{G}_0^{\sigma}]$. Inserting a vertex (or auxiliary spin) adds a new row and column to M_{σ}^{-1}. We imagine inserting this row and column on the border of the given matrix and write the resulting matrix in a block matrix form (omitting the σ index for simplicity):

$$[M^{(n+1)}]^{-1} = \begin{pmatrix} [M^{(n)}]^{-1} & Q \\ R & S \end{pmatrix}.$$

We furthermore define the analogous blocks of the M matrix as

$$M^{(n+1)} = \begin{pmatrix} \tilde{P} & \tilde{Q} \\ \tilde{R} & \tilde{S} \end{pmatrix}. \tag{8.38}$$

Here Q, R, and S are $n \times 1$, $1 \times n$, and 1×1 matrices that contain the functions $\mathcal{G}_0$ evaluated at time intervals determined by the position of the new vertex (spin). They can be easily computed. We want to find $\tilde{P}$, $\tilde{Q}$, $\tilde{R}$, $\tilde{S}$, and the ratio of determinants.

[14] In the following, we write the formulas without the tildes, that is, for the sampling of interaction vertices. For the algorithm with auxiliary spins, it suffices to replace $M \to \tilde{M}$ and $\mathcal{G}_0 \to \tilde{\mathcal{G}}_0$.

https://doi.org/10.1017/CBO9780511902581.009 Published online by Cambridge University Press

To do this we use the expression (7.49) for the block inversion of a matrix and (7.50) for the determinant of a block matrix. With the help of these formulas we can show that the determinant ratio needed for the acceptance probability is

$$\frac{\det[M^{(n+1)}]^{-1}}{\det[M^{(n)}]^{-1}} = \det(S - RM^{(n)}Q) = S - RM^{(n)}Q. \tag{8.39}$$

Because we store $M^{(n)}$, computing the acceptance probability of an insertion move is just an $\mathcal{O}(n^2)$ operation. If the move is accepted, we compute the new matrix $M^{(n+1)}$ from $M^{(n)}$, Q, R, and S, also in a time $\mathcal{O}(n^2)$:

$$\tilde{S} = (S - [R]\,[M^{(n)}\,Q])^{-1}, \tag{8.40}$$

$$\tilde{Q} = -[M^{(n)}Q]\,\tilde{S}, \tag{8.41}$$

$$\tilde{R} = -\tilde{S}\,[R\,M^{(n)}], \tag{8.42}$$

$$\tilde{P} = M^{(n)} + [M^{(n)}Q]\,\tilde{S}\,[RM^{(n)}]. \tag{8.43}$$

In the case of removing a spin we imagine removing a bordering row and column. It follows from (8.39) and (8.40) that

$$\frac{\det[M^{(n)}]^{-1}}{\det[M^{(n+1)}]^{-1}} = \det\tilde{S} = \tilde{S}. \tag{8.44}$$

$\tilde{S}$ is just a 1×1 matrix, so its determinant is trivial to compute. The above formulas also imply that the elements of the reduced matrix are

$$M^{(n)} = \tilde{P} - [\tilde{Q}][\tilde{R}]/\tilde{S}. \tag{8.45}$$

The calculation of the removal probability is thus $\mathcal{O}(1)$, while the calculation of the new $M^{(n)}$ matrix is $\mathcal{O}(n^2)$.

Algorithm 28 describes the elementary updates in the weak-coupling approach, namely, the insertion and removal of a spin, and shows how the fast matrix update formulas are used within these procedures.

8.4.3 Measurement of the Green's function

To compute the contribution of a configuration C to the Green's function, $G_C^\sigma(\tau)$, we insert in the right-hand side of (8.30) a creation operator $d^\dagger$ at time 0 and an annihilation operator d at time τ and divide by w_C. Wick's theorem and (8.39) then lead to the expression (Rubtsov et al., 2005)

$$G_C^\sigma(\tau) = \mathcal{G}_0^\sigma(\tau) - \sum_k \mathcal{G}_0^\sigma(\tau - \tau_k) \sum_l [M_\sigma]_{kl} \mathcal{G}_0^\sigma(\tau_l). \tag{8.46}$$

Our estimate for the impurity Green's function for a given imaginary time then follows from (8.28). To avoid unnecessary and time-consuming summations during

https://doi.org/10.1017/CBO9780511902581.009 Published online by Cambridge University Press

Algorithm 28 Vertex (spin) insertion/removal in the weak-coupling continuous-time impurity solver.

Input: Time-ordered spin configuration $C = \{(\tau_1, s_1), \ldots, (\tau_n, s_n)\}$, inverse Weiss Green's function matrix M, Weiss Green's function $\mathcal{G}_0$, interaction U, inverse temperature β.

```
Draw a uniform random number ζ ∈ [0, 1] ;
if (ζ < 0.5) then
    ▷ Try to insert a spin
  Randomly choose spin orientation s ;
  Randomly choose spin position τ ∈ [0, β) ;
  Compute acceptance probability A(n + 1 ← n) using (8.36) and (8.39) ;
  Draw a uniform random number ζ′ ∈ [0, 1] ;
  if (ζ′ < A(n + 1 ← n)) then
    Insert (τ, s) into C ;
    Update M using G_0 and (8.40)–(8.43) ;
  end if
else if (n > 0) then
    ▷ Try to remove a spin
  Randomly choose one of the spins in C ;
  Compute acceptance probability A(n − 1 ← n) using (8.37) and (8.44) ;
  Draw a uniform random number ζ′ ∈ [0, 1] ;
  if (ζ′ < A(n − 1 ← n)) then
    Remove the chosen spin from C ;
    Update M using (8.45).
  end if
end if
return the updated C and M.
```

the Monte Carlo simulation (evaluation of (8.46) for many τ-values), we accumulate the quantity (Gull et al., 2008)

$$S_\sigma(\tilde{\tau}) \equiv \sum_k \delta(\tilde{\tau} - \tau_k) \sum_l \left[M_\sigma\right]_{kl} \mathcal{G}_0^\sigma(\tau_l),$$

by binning the time points $\tilde{\tau}$ on a fine grid. After the simulation is finished, we compute the Green's function as[15]

$$G^\sigma(\tau) = \mathcal{G}_0^\sigma(\tau) - \int_0^\beta d\tilde{\tau}\, \mathcal{G}_0^\sigma(\tau - \tilde{\tau}) \left\langle S_\sigma(\tilde{\tau}) \right\rangle_{\mathrm{MC}}. \tag{8.47}$$

[15] Comparison of this equation with the impurity Dyson equation $G = \mathcal{G}_0 + \mathcal{G}_0 \star \Sigma \star G$ (where the $\star$ symbol denotes a convolution in imaginary time) shows that his procedure amounts to measuring $-\Sigma \star G$.

https://doi.org/10.1017/CBO9780511902581.009 Published online by Cambridge University Press

It is also possible to measure the Matsubara components of the Green's function directly. Using the imaginary-time translational invariance of the Green's functions, we obtain

$$G_C^\sigma(i\omega_n) = \mathcal{G}_0^\sigma(i\omega_n) - \mathcal{G}_0^\sigma(i\omega_n) \sum_{kl} \frac{1}{\beta} e^{i\omega_n(\tau_k - \tau_l)} [M_\sigma]_{kl} \mathcal{G}_0^\sigma(i\omega_n),$$

so that

$$G^\sigma(i\omega_n) = \mathcal{G}_0^\sigma(i\omega_n) - \frac{1}{\beta}(\mathcal{G}_0^\sigma(i\omega_n))^2 \left\langle \sum_{kl} e^{i\omega_n(\tau_k - \tau_l)} [M_\sigma]_{kl} \right\rangle_{\mathrm{MC}}. \tag{8.48}$$

We note that because the Weiss Green's function has the high-frequency behavior $\mathcal{G}_0(i\omega_n) \sim 1/i\omega_n$, the measured impurity Green's function automatically inherits the correct high-frequency tail.

8.4.4 Multi-orbital and cluster impurity problems

The generalization of the weak-coupling method to impurity clusters is straightforward. All we have to do is to add a site index to the interaction vertices (or auxiliary Ising spin variables) and sample the vertices (auxiliary spins) on a family of n_{sites} imaginary-time intervals. In principle, we could even use the weak-coupling solver to simulate lattice models by making the cluster size the size of the lattice.[16] However, as discussed in Section 7.3, the $\mathcal{O}(n_{\mathrm{sites}}^3 \beta^3)$ scaling of the computational effort is not competitive with the $\mathcal{O}(n_{\mathrm{sites}}^3 \beta)$ scaling of the BSS determinant method.[17]

General four-Fermion terms as in (8.4) are, at least in principle, also easily dealt with. We simply expand the partition function in powers of the interactions U^{abcd}. The trace over the impurity and bath degrees of freedom again yields a determinant of a matrix whose order equals the total perturbation order. In general there is a sign problem. To reduce the sign problem, it is advantageous to introduce auxiliary fields α and replace

$$\frac{1}{2} \sum_{abcd} U^{abcd} d_a^\dagger d_b^\dagger d_c d_d \to -\frac{1}{2} \sum_{abcd} U^{abcd} (d_a^\dagger d_c - \alpha_{ac})(d_b^\dagger d_d - \alpha_{bd}),$$

with an appropriate shift in the quadratic part of the Hamiltonian. However, in general, we cannot completely eliminate the sign problem by a suitable choice of α parameters. Furthermore, because the number of interaction terms grows like $\mathcal{O}(n_{\mathrm{orbitals}}^4)$, the computational cost rapidly escalates. In practice, the strong-coupling approach we discuss next is a more suitable approach for single-site multi-orbital problems with general interactions.

[16] Rombouts et al. (1999b) proposed such an algorithm in a pioneering work that introduced the idea of a determinant-based continuous-time Monte Carlo sampling for Fermion systems.

[17] In Appendix M we discuss a more suitable lattice Monte Carlo method that combines the weak-coupling continuous-time approach with elements of the determinant algorithm of Chapter 7, and thereby recovers the linear-in-β scaling.

https://doi.org/10.1017/CBO9780511902581.009 Published online by Cambridge University Press

8.5 Strong-coupling approach

While the Monte Carlo weights in the weak-coupling method are expressed in terms of the Weiss Green's function $\mathcal{G}_0$, the strong coupling method, which is in many ways complementary to the weak-coupling approach, naturally involves the hybridization function Δ. It follows from (8.15) that the Weiss Green's function and hybridization function contain the same information, and the DMFT procedure sketched in Algorithm 26 could be written just as well as a self-consistency loop fixing the hybridization function Δ.

The strong-coupling approach (Werner et al., 2006) is based on an expansion of the partition function in powers of the impurity-bath hybridization term.[18] Here, we decompose the Hamiltonian as $H_2 = H_{\text{mix}}$ and $H_1 = H - H_2 = H_\mu + H_U + H_{\text{bath}}$. Because $H_2 \equiv H_2^{d^\dagger} + H_2^d = \sum_{p\sigma} V_{p\sigma} d_\sigma^\dagger c_{p\sigma} + \sum_{p\sigma} V_{p\sigma}^* c_{p\sigma}^\dagger d_\sigma$ has two terms, corresponding to electrons hopping from the bath to the impurity and from the impurity back to the bath, only even perturbation orders contribute to (8.29). Furthermore, at perturbation order $2n$, only the $(2n)!/(n!)^2$ terms corresponding to n creation operators $d^\dagger$ and n annihilation operators d contribute. We therefore write the partition function as a sum over configurations $\{\tau_1, \ldots, \tau_n; \tau_1', \ldots, \tau_n'\}$ that are collections of imaginary-time points corresponding to these n annihilation and n creation operators:

$$Z = \sum_{n=0}^{\infty} \int_0^\beta d\tau_1 \cdots \int_{\tau_{n-1}}^\beta d\tau_n \int_0^\beta d\tau_1' \cdots \int_{\tau_{n-1}'}^\beta d\tau_n' \times \operatorname{Tr}\Big[e^{-\beta H_1} \mathcal{T} H_2^d(\tau_n) H_2^{d^\dagger}(\tau_n') \cdots H_2^d(\tau_1) H_2^{d^\dagger}(\tau_1') \Big]. \tag{8.49}$$

Because the imaginary-time evolution operator $e^{-\tau H_1}$ does not rotate the spin in the case of the Anderson impurity model, the configurations must contain an equal number of creation and annihilation operators for each spin. Taking this additional constraint into account and using the explicit expressions for H_2^d and $H_2^{d^\dagger}$, we find

$$\begin{aligned} Z = Z_{\text{bath}} \sum_{\{n_\sigma\}} \prod_\sigma \int_0^\beta d\tau_1^\sigma \cdots \int_{\tau_{n_\sigma-1}^\sigma}^\beta d\tau_{n_\sigma}^\sigma \int_0^\beta d\tau_1'^\sigma \ldots \int_{\tau_{n_\sigma-1}'^\sigma}^\beta d\tau_{n_\sigma}'^\sigma \\ \times \operatorname{Tr}_d \Big[e^{-\beta H_{\text{loc}}} \mathcal{T} \prod_\sigma d_\sigma(\tau_{n_\sigma}^\sigma) d_\sigma^\dagger(\tau_{n_\sigma}'^\sigma) \ldots d_\sigma(\tau_1^\sigma) d_\sigma^\dagger(\tau_1'^\sigma) \Big] \\ \times \frac{1}{Z_{\text{bath}}} \operatorname{Tr}_c \Big[e^{-\beta H_{\text{bath}}} \mathcal{T} \prod_\sigma \sum_{p_1 \ldots p_{n_\sigma}} \sum_{p_1' \ldots p_{n_\sigma}'} V_{p_1\sigma}^* V_{p_1'\sigma} \cdots V_{p_{n_\sigma}\sigma}^* V_{p_{n_\sigma}'\sigma} \\ c_{p_{n_\sigma}\sigma}^\dagger(\tau_{n_\sigma}^\sigma) c_{p_{n_\sigma}'\sigma}(\tau_{n_\sigma}'^\sigma) \ldots c_{p_1\sigma}^\dagger(\tau_1^\sigma) c_{p_1'\sigma}(\tau_1'^\sigma) \Big], \end{aligned}$$

[18] The technically correct term is therefore *hybridization expansion* approach, rather than strong-coupling approach, but we will use both terms interchangeably.

https://doi.org/10.1017/CBO9780511902581.009 Published online by Cambridge University Press

where to separate the d and c operators we used the fact that H_1 does not mix the impurity and the bath. The local Hamiltonian $H_{\rm loc}$ is defined in (8.7) and $Z_{\rm bath} = \mathrm{Tr}_c[e^{-\beta H_{\rm bath}}]$.

Introducing the β-antiperiodic hybridization function (8.14), which in the time domain reads

$$\Delta^\sigma(\tau) = \sum_p \frac{|V_{p\sigma}|^2}{e^{\varepsilon_p\beta}+1} \begin{cases} -e^{-\varepsilon_p(\tau-\beta)} & 0<\tau<\beta \\ e^{-\varepsilon_p\tau} & -\beta<\tau<0 \end{cases},$$

we reexpress the trace over the bath states as

$$\frac{1}{Z_{\rm bath}}\mathrm{Tr}_c\Big[e^{-\beta H_{\rm bath}}\mathcal{T}\prod_\sigma \sum_{p_1\dots p_{n_\sigma}}\sum_{p'_1\dots p'_{n_\sigma}} V^*_{p_1\sigma}V_{p'_1\sigma}\cdots V^*_{p_{n_\sigma}\sigma}V_{p'_{n_\sigma}\sigma} \\ c^\dagger_{p_{n_\sigma}\sigma}(\tau^\sigma_{n_\sigma})c_{p'_{n_\sigma}\sigma}(\tau'^\sigma_{n_\sigma})\dots c^\dagger_{p_1\sigma}(\tau^\sigma_1)c_{p'_1\sigma}(\tau'^\sigma_1)\Big] = \prod_\sigma \det M^{-1}_\sigma,$$

where M^{-1}_σ is the $(n_\sigma \times n_\sigma)$ matrix with elements

$$[M^{-1}_\sigma]_{ij} = \Delta^\sigma(\tau'^\sigma_i - \tau^\sigma_j).$$

In the hybridization expansion approach, the configuration space consists of all sequences $C = \{\tau^\uparrow_1,\dots,\tau^\uparrow_{n_\uparrow};\tau'^\uparrow_1,\dots,\tau'^\uparrow_{n_\uparrow}|\tau^\downarrow_1,\dots,\tau^\downarrow_{n_\downarrow};\tau'^\downarrow_1,\dots,\tau'^\downarrow_{n_\downarrow}\}$ of $n_\uparrow$ creation and annihilation operators for spin up ($n_\uparrow = 0,1,\dots$) and $n_\downarrow$ creation and annihilation operators for spin down ($n_\downarrow = 0,1,\dots$). The weight of this configuration is

$$w_C = Z_{\rm bath}\mathrm{Tr}_d\Big[e^{-\beta H_{\rm loc}}\mathcal{T}\prod_\sigma d_\sigma(\tau^\sigma_{n_\sigma})d^\dagger_\sigma(\tau'^\sigma_{n_\sigma})\cdots d_\sigma(\tau^\sigma_1)d^\dagger_\sigma(\tau'^\sigma_1)\Big] \\ \times\prod_\sigma \det M^{-1}_\sigma (d\tau)^{2n_\sigma}. \tag{8.50}$$

The trace factor represents the contribution of the impurity, which fluctuates between different quantum states as electrons hop in and out. The determinants sum up all bath evolutions that are compatible with the given sequence of transitions. We discuss the importance of this summation in Section 8.7.

To evaluate the trace factor, we may, for example, use the eigenbasis of $H_{\rm loc}$. In this basis, the imaginary-time evolution operator $e^{-\tau H_{\rm loc}}$ is diagonal, while the operators d_σ and $d^\dagger_\sigma$ produce transitions between eigenstates with amplitude ± 1. Because the time evolution does not flip the electron spin, the creation and annihilation operators for a given spin alternate. This observation allows us to separate the operators for spin up from those for spin down and to depict the time evolution by

https://doi.org/10.1017/CBO9780511902581.009 Published online by Cambridge University Press

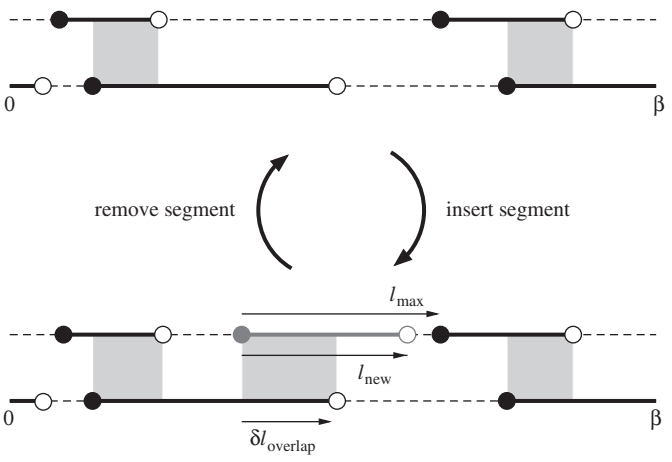

Figure 8.6 Local update in the segment picture. The two segment configurations correspond to spin-up and-down electrons. Each segment depicts a time interval in which an electron of the corresponding spin resides on the impurity. The segment end points are the locations of the operators $d^\dagger$ (full circles) and d (empty circles). We increase the perturbation order by adding a segment or antisegment of random length for random spin and decrease it by removing a randomly chosen segment or antisegment.

a *collection of segments* with each segment representing an imaginary-time interval in which an electron of spin up or down resides on the impurity (Fig. 8.6). We call an unoccupied time interval between two segments an "antisegment."

At each time, the eigenstate of the impurity follows immediately from the segment representation, and the trace factor becomes

$$\mathrm{Tr}_d\left[e^{-\beta H_{\mathrm{loc}}}\mathcal{T}\prod_\sigma d_\sigma(\tau^\sigma_{n_\sigma})d^\dagger_\sigma(\tau'^\sigma_{n_\sigma})\cdots d_\sigma(\tau^\sigma_1)d^\dagger_\sigma(\tau'^\sigma_1)\right] = \mathcal{S}\exp\left[\mu(l_\uparrow + l_\downarrow) - U l_{\mathrm{overlap}}\right],$$

with $\mathcal{S}$ being a permutation sign, l_σ the total "length" of the segments for spin σ, and l_{overlap} the total length of the overlap between up and down segments. The lower panel of Fig. 8.6 shows a configuration with three segments for spin up and two segments for spin down. The time intervals where segments overlap, indicated by gray rectangles, correspond to a doubly occupied impurity and cost a repulsion energy U.

In the segment formalism, it is natural to decompose a configuration with zero segments (for a given spin σ) into the "full line" and "empty line" contributions corresponding to the occupied and empty σ states.

https://doi.org/10.1017/CBO9780511902581.009 Published online by Cambridge University Press

8.5.1 Sampling

For ergodicity, it is sufficient to insert and remove pairs of creation and annihilation operators (segments or antisegments) for spin up and down. One possible strategy for inserting a segment is the following: We select a random time in $[0, \beta)$ for the creation operator. If it falls on an existing segment, the impurity is already occupied and the move is rejected. If it falls on an empty space, we compute $l_{\max}$, the length from this selected time to the next segment (in the direction of increasing τ).[19] Then we choose the position of the new annihilation operator randomly in this interval of length $l_{\max}$ (Fig. 8.6). If in the inverse procedure we propose to remove a randomly chosen segment for this spin, then the proposal probabilities for the insertion and removal are

$$T(n_\sigma + 1 \leftarrow n_\sigma) = \frac{d\tau}{\beta}\frac{d\tau}{l_{\max}}, \qquad T(n_\sigma \leftarrow n_\sigma + 1) = \frac{1}{n_\sigma + 1}.$$

The acceptance probability for the insertion of a segment becomes $A(n_\sigma + 1 \leftarrow n_\sigma) = \min[1, \mathcal{R}_{\text{insert}}(n_\sigma + 1 \leftarrow n_\sigma)]$, with

$$\mathcal{R}_{\text{insert}}(n_\sigma + 1 \leftarrow n_\sigma) = \frac{\beta l_{\max}}{n_\sigma + 1} e^{\mu l_{\text{new}} - U\delta l_{\text{overlap}}} \frac{\det\left[M_\sigma^{(n_\sigma+1)}\right]^{-1}}{\det\left[M_\sigma^{(n_\sigma)}\right]^{-1}}, \tag{8.51}$$

while the acceptance probability for a removal is obtained from

$$\mathcal{R}_{\text{remove}}(n_\sigma \leftarrow n_\sigma + 1) = 1/\mathcal{R}_{\text{insert}}(n_\sigma + 1 \leftarrow n_\sigma). \tag{8.52}$$

Here, l_{new} is the length of the new segment, and $\delta l_{\text{overlap}}$ is the change in the overlap. Again, we compute the ratio of determinants using the fast update formulas discussed in Section 8.4.2. Algorithm 29 describes the steps needed for the insertion or removal of a segment. Analogous procedures are used for the insertion or removal of antisegments.[20]

8.5.2 Measurement of the Green's function

The strategy is to create configurations that contribute to the Green's function measurement by decoupling the bath from a given pair of creation and annihilation operators in a configuration C. We start by expressing the expectation value for the Green's function as

$$G(\tau) = -\frac{1}{Z}\sum_C w_C^{d(\tau)d^\dagger(0)} = -\frac{1}{Z}\sum_C w_C^{(\tau,0)} \frac{w_C^{d(\tau)d^\dagger(0)}}{w_C^{(\tau,0)}},$$

[19] If there are no segments for the given spin, $l_{\max} = \beta$.
[20] At order $n_\sigma = 1$, the removal of the antisegment leads to a full line.

https://doi.org/10.1017/CBO9780511902581.009 Published online by Cambridge University Press

Algorithm 29 Insertion/removal of a segment in the strong-coupling continuous-time impurity solver.

Input: Configuration $C = \{(\tau_1'^{\uparrow}, \tau_1^{\uparrow}), \ldots, (\tau_{n_\uparrow}'^{\uparrow}, \tau_{n_\uparrow}^{\uparrow}); (\tau_1'^{\downarrow}, \tau_1^{\downarrow}), \ldots, (\tau_{n_\downarrow}'^{\downarrow}, \tau_{n_\downarrow}^{\downarrow})\}$, which at order $n_\sigma = 0$ encodes full or empty line, inverse hybridization function matrices M_σ, hybridization functions Δ_σ, interaction U, chemical potential μ, inverse temperature β.

Randomly choose the spin σ ;
Draw a uniform random number $\zeta \in [0, 1]$;
if $(\zeta < 0.5)$ **then**
  ▷ Try to insert a segment of spin σ
  Randomly choose the start time $\tau_\sigma' \in [0, \beta)$ for the new segment ;
  if τ_σ' does not lie on a spin-σ segment or full line of C **then**
    Compute length $l_{\max}$ to the next spin-σ creation operator ; ▷ Must consider periodic boundary conditions
    Randomly choose the end point τ_σ of the new segment in the interval of length $l_{\max}$ starting at τ_σ' ;
    Compute the length l_{new} of the new segment $(\tau_\sigma', \tau_\sigma)$;
    Compute the overlap $\delta l_{\text{overlap}}$ of the new segment $(\tau_\sigma', \tau_\sigma)$ with the segments of opposite spin ;
    Compute $A(n_\sigma + 1 \leftarrow n_\sigma)$ using (8.51) and (8.39) ;
    Draw a uniform random number $\zeta' \in [0, 1]$;
    if $(\zeta' < A(n_\sigma + 1 \leftarrow n_\sigma))$ **then**
      Insert the segment $(\tau_\sigma', \tau_\sigma)$ into C ;
      Update M_σ using Δ^σ and (8.40)–(8.43) ;
    end if
  end if
else if $(n_\sigma > 0)$ **then**
  ▷ Try to remove a segment of spin σ
  Randomly choose one of the segments of spin σ in C ;
  Compute the length of this segment ;
  Compute the overlap of this segment with segments of opposite spin ;
  Compute $A(n_\sigma - 1 \leftarrow n_\sigma)$ using (8.52) and (8.44) ;
  Draw a uniform random number $\zeta' \in [0, 1]$;
  if $(\zeta' < A(n_\sigma - 1 \leftarrow n_\sigma))$ **then**
    Remove the chosen segment from C ;
    Update M_σ using (8.45).
  end if
end if
return the updated C and M.

https://doi.org/10.1017/CBO9780511902581.009 Published online by Cambridge University Press

where $w_C^{d(\tau)d^\dagger(0)}$ denotes the weight of the configuration C with an additional operator $d^\dagger(0)$ and $d(\tau)$ in the trace factor, and $w_C^{(\tau,0)}$ denotes the complete weight corresponding to the enlarged operator sequence (including enlarged hybridization determinants). Because the trace factors of both weights are identical, up to a permutation sign $(-1)^{i+j}$,

$$\frac{w_C^{d(\tau)d^\dagger(0)}}{w_C^{(\tau,0)}} = \frac{(-1)^{i+j}\det\left[M_C\right]^{-1}}{\det\left[M_C^{(\tau,0)}\right]^{-1}} = \left[M_C^{(\tau,0)}\right]_{ji},$$

with i and j denoting the row and column corresponding to the additional operators $d^\dagger$ and d in the enlarged $[M_C^{(\tau,0)}]^{-1}$. Hence, the measurement formula for the Green's function becomes[21]

$$\begin{aligned} G(\tau) &= -\frac{1}{Z}\sum_C w_C^{(\tau,0)}[M_C^{(\tau,0)}]_{ji} = -\frac{1}{Z}\sum_{\tilde{C}} w_{\tilde{C}}\tilde{n}^2\delta(\tau_{\tilde{n}}-\tau)\delta(\tau'_{\tilde{n}}-0)[M_{\tilde{C}}]_{\tilde{n}\tilde{n}} \\ &= -\frac{1}{Z}\sum_{\tilde{C}} w_{\tilde{C}}\tilde{n}^2\frac{1}{\beta}\delta(\tau,\tau_{\tilde{n}}-\tau'_{\tilde{n}})[M_{\tilde{C}}]_{\tilde{n}\tilde{n}}, \end{aligned}$$

with $\delta(\tau,\tau') = \delta(\tau-\tau')$ for $\tau' > 0$, and $\delta(\tau,\tau') = -\delta(\tau-\tau'-\beta)$ for $\tau' < 0$. In the first step, we went from a sum over configurations C with n creation and annihilation operators in addition to $d(\tau)$ and $d^\dagger(0)$ to a sum over configurations $\tilde{C}$ with $\tilde{n} = n+1$ operator pairs, while in the last step, we used the translational invariance and the β-antiperiodicity of the Green's function. We finally replace the factor $\tilde{n}^2$ (which comes from the $1/(n!)^2$ factor in the Monte Carlo weights without time ordering) by a sum over all pairs i,j of creation and annihilation operators, to obtain the measurement formula $G(\tau) = -\frac{1}{Z}\sum_{\tilde{C}} w_{\tilde{C}} \sum_{ij} \frac{1}{\beta}\delta(\tau,\tau_j-\tau'_i)[M_{\tilde{C}}]_{ji}$, or

[21] For the purpose of this derivation, it is convenient to use configurations C and $\tilde{C}$ without time ordering, that is, we write the Green's function as

$$\begin{aligned} G(\tau) =& -\frac{Z_{\text{bath}}}{Z}\sum_n \frac{1}{n!^2}\int_0^\beta d\tau_1\cdots d\tau_n\int_0^\beta d\tau'_1\cdots d\tau'_n \\ &\times \mathrm{Tr}_d\left[e^{-\beta H_{\text{loc}}}\mathcal{T}d(\tau)d^\dagger(0)d(\tau_n)d^\dagger(\tau'_n)\cdots d(\tau_1)d^\dagger(\tau'_1)\right]\det\left[M^{(\tau,0)}\right]^{-1}\left[M^{(\tau,0)}\right]_{n+1,n+1} \\ =& -\frac{Z_{\text{bath}}}{Z}\sum_n \frac{(n+1)^2}{(n+1)!^2}\int_0^\beta d\tau_1\cdots d\tau_{n+1}\int_0^\beta d\tau'_1\cdots d\tau'_{n+1}\delta(\tau_{n+1}-\tau)\delta(\tau'_{n+1}-0) \\ &\times \mathrm{Tr}_d\left[e^{-\beta H_{\text{loc}}}\mathcal{T}d(\tau_{n+1})d^\dagger(\tau'_{n+1})d(\tau_n)d^\dagger(\tau'_n)\cdots d(\tau_1)d^\dagger(\tau'_1)\right]\det\left[M^{(\tau,0)}\right]^{-1}\left[M^{(\tau,0)}\right]_{n+1,n+1} \\ =& -\frac{Z_{\text{bath}}}{Z}\sum_{\tilde{n}} \frac{\tilde{n}^2}{(\tilde{n}!)^2}\int_0^\beta d\tau_1\cdots d\tau_{\tilde{n}}\int_0^\beta d\tau'_1\cdots d\tau'_{\tilde{n}}\delta(\tau_{\tilde{n}}-\tau)\delta(\tau'_{\tilde{n}}-0) \\ &\times \mathrm{Tr}_d\left[e^{-\beta H_{\text{loc}}}\mathcal{T}d(\tau_{\tilde{n}})d^\dagger(\tau'_{\tilde{n}})\cdots d(\tau_1)d^\dagger(\tau'_1)\right]\det\left[M^{(\tilde{n})}\right]^{-1}\left[M^{(\tilde{n})}\right]_{\tilde{n}\tilde{n}}. \end{aligned}$$

https://doi.org/10.1017/CBO9780511902581.009 Published online by Cambridge University Press

$$G(\tau) = \left\langle -\sum_{ij} \frac{1}{\beta} \delta(\tau, \tau_i - \tau_j') M_{ij} \right\rangle_{\mathrm{MC}} . \tag{8.53}$$

Fourier transformation of (8.53) yields the measurement formula

$$G(i\omega_n) = \left\langle -\sum_{ij} \frac{1}{\beta} e^{i\omega_n(\tau_i - \tau_j')} M_{ij} \right\rangle_{\mathrm{MC}} \tag{8.54}$$

for the Fourier coefficients of the Green's function. Note that in contrast to the weak-coupling approach, where we measure the Green's function as a $\mathcal{O}(1/(i\omega_n)^2)$ correction to the Weiss Green's function, (8.54) does not automatically yield the correct high-frequency tail.

An elegant way to suppress the noise in $G(i\omega_n)$ at large ω_n and to obtain a compact representation of the Green's function is to measure the expansion coefficients in a basis of orthogonal polynomials (Boehnke et al., 2011). A suitable choice are the *Legendre polynomials* $P_l(x)$ defined on $x \in [-1, 1]$ through the recursion relation

$$\begin{aligned} P_0(x) &= 1, \\ P_1(x) &= x, \\ (l+1)P_{l+1}(x) &= (2l+1)xP_l(x) - lP_{l-1}(x). \end{aligned}$$

The P_l furthermore satisfy $\int_{-1}^{1} dx P_k(x) P_l(x) = \frac{2}{2l+1}\delta_{kl}$. Defining $x(\tau) = 2\tau/\beta - 1$, we may thus express the Green's function on the interval $\tau \in [0, \beta]$ as

$$G(\tau) = \sum_{l \geq 0} \frac{\sqrt{2l+1}}{\beta} P_l(x(\tau)) G_l, \tag{8.55}$$

$$G_l = \sqrt{2l+1} \int_0^\beta d\tau P_l(x(\tau)) G(\tau). \tag{8.56}$$

The advantage of the Legendre representation over the Matsubara representation is a much faster decay of the expansion coefficients with increasing order. The Matsubara Fourier transform requires anti periodization of the Green's function with discontinuities at $\tau = m\beta$, which leads to slowly decaying Matsubara coefficients ($G(i\omega_n) \sim 1/i\omega_n$ for large ω_n). On the other hand, the Legendre basis represents the smooth function $G(\tau)$ on the interval $[0, \beta]$. In practice, 30–50 Legendre coefficients are enough to reproduce the Green's function with high precision, and neglecting the higher orders acts as a convenient noise filter.

From (8.53) and (8.56) it follows that

$$G_l = \left\langle -\sum_{ij} \frac{\sqrt{2l+1}}{\beta} \tilde{P}_l(\tau_i - \tau_j') M_{ij} \right\rangle_{\mathrm{MC}} , \tag{8.57}$$

with $\tilde{P}_l(\tau) = P_l(x(\tau))$ for $\tau > 0$ and $\tilde{P}_l(\tau) = -P_l(x(\tau + \beta))$ for $\tau < 0$.

https://doi.org/10.1017/CBO9780511902581.009 Published online by Cambridge University Press

The Matsubara coefficients are obtained from the Legendre coefficients as $G(i\omega_n) = \sum_{l\geq 0} T_{nl} G_l$, with the unitary transformation T_{nl} given by $T_{nl} = (-1)^n i^{l+1} \sqrt{2l+1} j_l(\frac{1}{2}\beta\omega_n)$ involving the spherical Bessel functions $j_l(z)$. In the limit $n \to \infty$, T_{nl} decays $\sim 1/(i\omega_n)$ for n even and $\sim 1/(i\omega_n)^2$ for n odd.

8.5.3 Generalization – Matrix formalism

It is obvious from the derivation in Section 8.5 that the hybridization expansion formalism is applicable to general classes of impurity models (Werner and Millis, 2006). Because we compute the trace factor in the weight (8.50) exactly, $H_{\rm loc}$ can contain arbitrary local interactions (e.g., spin-exchange terms in multi-orbital models), degrees of freedom (e.g., spins in Kondo-lattice models), or constraints (e.g., "no double occupancy" in the t-J model).

For multi-orbital impurity models with $H_{\rm loc}$ diagonal in the occupation number basis, such as models with density-density interactions, the segment formalism illustrated in Fig. 8.6 is still applicable. We now have a collection of segments for each *flavor* α (orbital, spin, etc.), and we still compute the trace factor from the length of the segments (the chemical potential contribution) and the overlaps between segments of different flavor (the interaction contribution). This allows a very efficient simulation of models with five, seven, and in principle even more orbitals, despite the fact that the corresponding Hilbert spaces ($4^5 = 1024$ for five orbitals, $4^7 = 16,384$ for seven orbitals) are quite large.

If $H_{\rm loc}$ is not diagonal in the occupation number basis defined by the $d^\dagger_\alpha$, the calculation of

$$\mathrm{Tr}_d \left[e^{-\beta H_{\rm loc}} \mathcal{T} \prod_\alpha d_\alpha(\tau^\alpha_{n_\alpha}) d^\dagger_\alpha(\tau'^\alpha_{n_\alpha}) \cdots d_\alpha(\tau^\alpha_1) d^\dagger_\alpha(\tau'^\alpha_1) \right] \tag{8.58}$$

becomes rather involved and for a model with a large Hilbert space also computationally expensive. An obvious idea is to evaluate the trace in the eigenbasis where the imaginary-time evolution operators $e^{-H_{\rm loc}\tau}$ become diagonal. On the other hand, the operators d_α and $d^\dagger_\alpha$, which are simple and sparse in the occupation number basis, become complicated matrices in the eigenbasis. The evaluation of the trace factor in the eigenbasis thus involves the multiplication of matrices whose size scales as the dimension of the Hilbert space of the local problem. Because the dimension of this Hilbert space grows *exponentially* with the number of flavors, the calculation of the trace factor becomes the computational bottleneck of the simulation, and the matrix formalism is therefore restricted to a relatively small number of flavors.

It is important to identify and use *conserved quantities* (Haule, 2007). Typically, these are particle number for spin up and spin down and momentum. If we

https://doi.org/10.1017/CBO9780511902581.009 Published online by Cambridge University Press

group the eigenstates of $H_{\rm loc}$ according to these quantum numbers, the operator matrices acquire a sparse block structure. For example, the operator $d^\dagger_{\uparrow,q}$ connects states corresponding to the quantum numbers $m = \{n_\uparrow, n_\downarrow, k, \ldots\}$ to those with $m' = \{n_\uparrow + 1, n_\downarrow, k + q, \ldots\}$ (if they exist). Checking the compatibility of the operator sequence with the different starting blocks allows us to identify the blocks that contribute to the trace without performing any expensive matrix-matrix multiplications.

Let us take as a simple example a two-orbital model with conserved quantum numbers $n_\uparrow$ and $n_\downarrow$. The operator sequence $d^\dagger_\uparrow(\tau_4)d^\dagger_\uparrow(\tau_3)d_\uparrow(\tau_2)d_\uparrow(\tau_1)$ (with $\tau_1 < \tau_2 < \tau_3 < \tau_4$) is compatible with the starting blocks $\{n_\uparrow = 2; n_\downarrow = 0, 1, 2\}$, since the quantum numbers evolve as

$$\{n_\uparrow = 2; n_\downarrow\} \underset{d_\uparrow}{\rightarrow} \{n_\uparrow = 1; n_\downarrow\} \underset{d_\uparrow}{\rightarrow} \{n_\uparrow = 0; n_\downarrow\} \underset{d^\dagger_\uparrow}{\rightarrow} \{n_\uparrow = 1; n_\downarrow\} \underset{d^\dagger_\uparrow}{\rightarrow} \{n_\uparrow = 2; n_\downarrow\},$$

whereas the blocks $\{n_\uparrow = 0, 1; n_\downarrow = 0, 1, 2\}$ do not contribute to the weight, since, for example,

$$\{n_\uparrow = 1; n_\downarrow\} \underset{d_\uparrow}{\rightarrow} \{n_\uparrow = 0; n_\downarrow\} \underset{d_\uparrow}{\rightarrow} \emptyset.$$

Having identified the contributing blocks, the trace calculation reduces to a block matrix multiplication of the form

$$\sum_{\substack{\text{contributing} \\ m}} \mathrm{Tr}_m \Big[\cdots [O]_{m''m'} [e^{-(\tau'-\tau)H_{\rm loc}}]_{m'} [O]_{m'm} [e^{-\tau H_{\rm loc}}]_m \Big], \tag{8.59}$$

where O is either a creation or an annihilation operator, m denotes the index of the matrix block, and the sum runs over those starting sectors that are compatible with the operator sequence.

Using the block structure imposed by the conserved quantum numbers, we can simulate three-orbital models or four-site clusters efficiently. However, because the matrix blocks are dense and the largest blocks grow exponentially with system size, the simulation of five-orbital models already becomes quite expensive, and the simulation of seven-orbital models with five, six, or seven electrons is doable only if we truncate the size of the blocks.

In fact, one should distinguish two types of truncations:

1. Restriction of the trace $\sum_{\text{contributing } m} \mathrm{Tr}_m[\ldots]$ to those quantum number sectors or states that give the dominant contribution
2. Reduction of the size of the operator blocks $[O]_{m'm''}$ by eliminating high-energy states.

https://doi.org/10.1017/CBO9780511902581.009 Published online by Cambridge University Press

Truncations of type 1 have little effect at low enough temperature, because they restrict the possible states only at a single point on the imaginary-time interval. Truncations of the type 2 are more problematic and possibly lead to systematic errors that are difficult to estimate and control when the system size is large.

Accumulating a histogram of the states or quantum number sectors visited during the sampling can be very instructive. For example, in the study of correlated materials with multiple partially filled orbitals, interesting issues are the typical valence or the dominant spin state, and the importance of fluctuations to other charge and spin states. Dynamical mean-field theory allows us to address these issues by adopting a real-space representation of the solid as a collection of atoms and treating the local fluctuations on a given site through the effective impurity model construction. The strong-coupling solver, which treats the local part of the impurity problem exactly, is ideally suited for such an analysis.

As an illustration, we show in Fig. 8.7 a histogram accumulated in a DMFT simulation of a half-filled two-orbital model (Werner and Millis, 2007). The energies of the two orbitals are shifted relative to each other by a "crystal field splitting" δ. For large δ, it is energetically favorable to put the two electrons into the lower orbital and hence into a low-spin ($S = 0$) configuration. For small δ, the Hund's

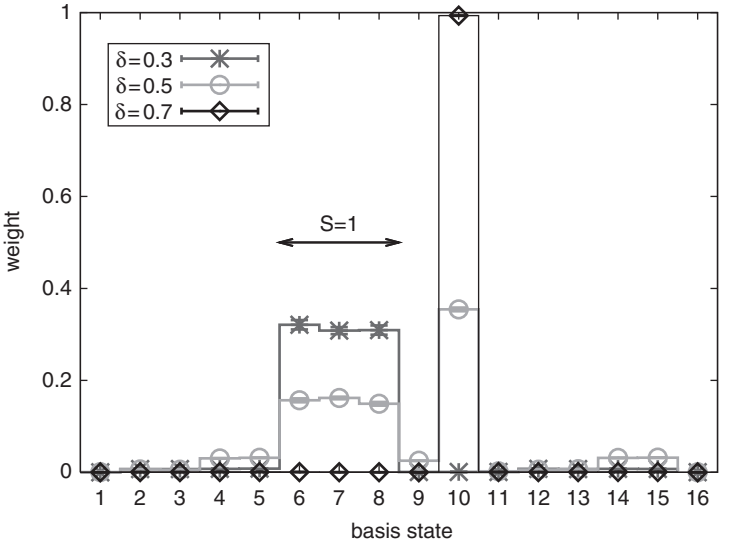

Figure 8.7 Histogram of local quantum states in a DMFT simulation of a half-filled two-orbital model with strong interactions and Hund's coupling, and with a crystal field splitting δ between the orbitals. The band widths are 4, and the temperature is $\frac{1}{50}$. The histogram shows the average relative contribution of each of the 16 eigenstates of H_{loc} to the weight of the Monte Carlo configurations. (Adapted from Werner and Millis (2007).)

https://doi.org/10.1017/CBO9780511902581.009 Published online by Cambridge University Press

interaction favors a high-spin ($S = 1$) state with equal occupation of both orbitals. At large interaction, we may thus anticipate a transition from a high-spin to a low-spin insulating phase, as the crystal field splitting δ increases, with possibly a metallic phase appearing in between. What is shown in the figure is the weight of the $4^2 = 16$ atomic states (eigenstates of $H_{\rm loc}$) or more precisely the average contribution of each of these states to the trace factor (8.58). We see that for the smallest crystal field splitting, three states ($|6\rangle$, $|7\rangle$, $|8\rangle$) dominate; these are the three degenerate, half-filled $S = 1$ states. The eigenstates $|10\rangle$ and $|11\rangle$ are linear combinations of the two states with two electrons in one orbital and none in the other, with state $|10\rangle$ having the lower energy. This half-filled, low-energy $S = 0$ state becomes the dominant state at large δ. Hence, by looking at the histogram of atomic states, we can immediately identify the high-spin and low-spin character of the two phases at small and large δ. Because they are insulating, fluctuations to other charge states are suppressed.

The histogram for the intermediate value of δ exhibits a different character. Here, the half-filled spin singlet and spin triplet states all contribute significantly to the trace, and charge fluctuations to states with one (e.g., $|4\rangle$, $|5\rangle$) or three (e.g., $|14\rangle$, $|15\rangle$) electrons are not negligible. This histogram corresponds to a metallic solution that appears close to the level-crossing of the half-filled high-spin and low-spin atomic states.

As this simple example shows, by looking at the state histogram and by identifying the dominant states and the degeneracies that appear in these histograms, we gain valuable insights into the nature of phases and phase transitions in the DMFT solution of complicated (multi-orbital) lattice models.

8.5.4 Generalization – Krylov formalism

An alternative strategy (Läuchli and Werner, 2009) to evaluate the trace factor (8.58) is to:

1. Adopt the occupation number basis in which we can easily apply the d_α and $d_\alpha^\dagger$ operator matrices to any state and in which we can exploit the sparse nature of $H_{\rm loc}$ during the imaginary-time evolutions
2. Approximate the trace by a sum over the lowest energy states, that is, by a truncation of type (1) described in the previous subsection.

Instead of evaluating the matrix corresponding to the product of operators, we propagate each retained state in the trace through the sequence of time-evolution, creation, and annihilation operators. This computation involves only matrix-vector multiplications of the type $d_\alpha|v\rangle$, $d_\alpha^\dagger|v\rangle$, and $H_{\rm loc}|v\rangle$ with *sparse* operators d_α, $d_\alpha^\dagger$, and $H_{\rm loc}$ and is thus possible for systems for which the multiplication of dense

https://doi.org/10.1017/CBO9780511902581.009 Published online by Cambridge University Press

matrix blocks becomes prohibitively expensive. Furthermore, the approach does not require any truncation of type (2), so all excited states remain accessible at intermediate τ. While the sparsity of H_{loc} depends on the number of interaction terms, this number grows at most proportionally to the number of orbitals squared. In contrast, the dimension of the matrix grows exponentially with the number of orbitals.

The expensive step is the calculation of the time evolution from one operator to the next. We evaluate the matrix exponentials applied to a vector, $\exp(-\tau H_{\mathrm{loc}})|v\rangle$, by iteratively constructing the *Krylov space*

$$\mathcal{K}_p(|v\rangle) = \mathrm{span}\{|v\rangle, H_{\mathrm{loc}}|v\rangle, H_{\mathrm{loc}}^2|v\rangle, \ldots, H_{\mathrm{loc}}^p|v\rangle\}$$

and by approximating the full matrix exponential by the matrix exponential of the Hamiltonian projected onto $\mathcal{K}_p(|v\rangle)$. The iteration number p is determined by tracking the convergence of $\exp(-\tau H_{\mathrm{loc}})|v\rangle$ and stopping the calculation if the difference between iteration p and $p+1$ drops below some cutoff value. The number of iterations depends on the time interval τ, but typically, convergence occurs for very small iteration numbers $p \ll N_{\mathrm{dim}}$, with N_{dim} the dimension of the Hilbert space.

In the limit where the dimension of the local Hilbert space N_{dim} is large, the Krylov approach is more efficient than an implementation based on a matrix representation of the operators d_α, $d_\alpha^\dagger$, and an evaluation of the trace of the matrix product. If the Monte Carlo configuration has n creation and n annihilation operators and we perform the trace over $N_{\mathrm{tr}} \leq N_{\mathrm{dim}}$ states, the Krylov calculation of the trace scales as

$$\mathcal{O}(N_{\mathrm{tr}} N_{\mathrm{dim}} 2n(1 + \langle p \rangle)),$$

where the first term comes from the application of the creation and annihilation operators and the second term, proportional to the average dimension $\langle p \rangle$ of the Krylov space, from the application of the time-evolution operators. If we retain all the states in the trace calculation, $N_{\mathrm{tr}} = N_{\mathrm{dim}}$, and the trace calculation scales as N_{dim}^2. If we restrict the trace to a small number of low-energy states, then N_{tr} is $\mathcal{O}(1)$ and the trace computation becomes *linear* in N_{dim}. This scaling should be compared with a computational effort of $\mathcal{O}(2nN_{\mathrm{dim}}^3)$ for the evaluation of the trace based on matrix multiplications (without truncation of the matrix blocks).[22]

While in theory the Krylov space approach is the method of choice due to its superior N_{dim} scaling, in practice, the precise numbers of N_{tr}, $\langle p \rangle$, and N_{dim} determine which one of the two approaches performs better for a given problem. Experience shows that for five-orbital problems the Krylov approach becomes superior to the matrix method.

[22] In the truncated trace approach, it is important to measure the various local observables at $\tau = \frac{1}{2}\beta$ where they are least affected by the truncation at $\tau = 0$ and $\tau = \beta$. Also, it is important not to destroy the multiplet structure when truncating the trace.

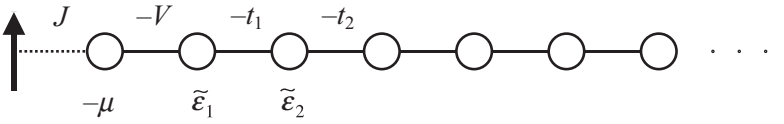

Figure 8.8 Chain representation of the quantum impurity model in the Kondo limit. The impurity states are restricted to the singly occupied states $|\uparrow\rangle$ and $|\downarrow\rangle$. This spin-$\frac{1}{2}$ degree of freedom couples via the exchange integral J to the spin $\vec{S} = \frac{1}{2}\psi_c^\dagger \vec{\sigma} \psi_c$ on lattice site 0, represented in the figure by the first site of the chain.

8.6 Infinite-U limit: Kondo model

In the limit of very strong interaction, we cannot efficiently simulate the half-filled Anderson impurity model using the weak- or strong-coupling continuous-time Monte Carlo solvers. The weak-coupling approach is unsuitable because the perturbation order becomes very large, and the strong-coupling approach may encounter a problem with the sampling efficiency, because hybridization events correspond to transitions into doubly occupied or empty states with very high energy. While transitions into states with occupancy different from unity are acceptable, as long as the excursion is very short-lived, and the strong-coupling algorithm in principle handles arbitrarily short segments or anti segments, it is more appropriate and more efficient to project out the charge fluctuations and consider a low-energy effective model in which the singly-occupied impurity (represented by a spin $\frac{1}{2}$) exchanges spin with the bath (Fig. 8.8). This projection from the Anderson impurity model leads us to the second iconic impurity model, the Kondo impurity model defined in (8.2). To solve this model, we have to compute the Green's function of the bath at site 0 (the location of the impurity). The Green's function of the impurity then follows from the T-matrix of the bath (Costi, 2000). In the following sections, we discuss two complementary continuous-time solvers for the Kondo impurity model: (i) the weak-coupling approach based on an expansion in powers of the exchange interaction J and (ii) the strong-coupling approach based on an expansion in powers of the hybridization V between the site 0 and the rest of the bath.

8.6.1 Weak-coupling approach

In the weak-coupling simulation (Otsuki et al., 2007), we Fermionize the local spin $\vec{s}$ by introducing creation operators $d_\sigma^\dagger$ and writing

$$\vec{s} = \frac{1}{2}\psi_d^\dagger \vec{\sigma} \psi_d,$$

with $\vec{\sigma} = (\sigma^x, \sigma^y, \sigma^z)$ and $\psi_d^\dagger = (d_\uparrow^\dagger, d_\downarrow^\dagger)$. We then express the Hamiltonian (8.2) with a wave-number-independent coupling J as

https://doi.org/10.1017/CBO9780511902581.009 Published online by Cambridge University Press

$$H = \sum_{k\sigma} \epsilon_k c^\dagger_{k\sigma} c_{k\sigma} + \frac{1}{2} J \Big[s^z (c^\dagger_\uparrow c_\uparrow - c^\dagger_\downarrow c_\downarrow) + s^+ c^\dagger_\downarrow c_\uparrow + s^- c^\dagger_\uparrow c_\downarrow \Big], \tag{8.60}$$

where $s^+ = d^\dagger_\uparrow d_\downarrow$, $s^- = d^\dagger_\downarrow d_\uparrow$, $s^z = \frac{1}{2}(d^\dagger_\uparrow d_\uparrow - d^\dagger_\downarrow d_\downarrow)$, and $c^\dagger_\sigma = \frac{1}{\sqrt{N}} \sum_k c^\dagger_{k\sigma}$ is the creation operator for conduction electrons at site 0 (the first site in the chain representation). Using the constraint $d^\dagger_\uparrow d_\uparrow + d^\dagger_\downarrow d_\downarrow = 1$, we rewrite the Hamiltonian again, to obtain

$$H = \sum_{k\sigma} \epsilon_k c^\dagger_{k\sigma} c_{k\sigma} - \frac{1}{4} J \sum_\sigma c^\dagger_\sigma c_\sigma + \frac{1}{2} J \sum_{\sigma\sigma'} d^\dagger_\sigma d_{\sigma'} c^\dagger_{\sigma'} c_\sigma. \tag{8.61}$$

For the weak-coupling simulation, we split this Hamiltonian into the exactly solvable part $H_1 = \sum_{k\sigma} \epsilon_k c^\dagger_{k\sigma} c_{k\sigma} - \frac{1}{4} J \sum_\sigma c^\dagger_\sigma c_\sigma$ and the remainder $H_2 = \frac{J}{2} \sum_{\sigma\sigma'} d^\dagger_\sigma d_{\sigma'} c^\dagger_{\sigma'} c_\sigma$ and then expand the partition function in powers of H_2. The trace over the Fermionic degrees of freedom yields the weight of the Monte Carlo configuration with perturbation order n and a given sequence of "diagonal" ($c^\dagger_\sigma c_\sigma$) and "off-diagonal" ($c^\dagger_\sigma c_{\bar\sigma}$) operators:

$$\begin{aligned} w_C = (-Jd\tau/2)^n \mathrm{Tr}_d \Big[\mathcal{T} d^\dagger_{\sigma_1}(\tau_1) d_{\sigma'_1}(\tau_1) \cdots d^\dagger_{\sigma_n}(\tau_n) d_{\sigma'_n}(\tau_n) \Big] \\ \times \prod_\sigma Z_c \frac{1}{Z_c} \mathrm{Tr}_c \Big[e^{-\beta H_1} \mathcal{T} c^\dagger_\sigma(\tau'_1) c_\sigma(\tau''_1) \cdots c^\dagger_\sigma(\tau'_{n_\sigma}) c_\sigma(\tau''_{n_\sigma}) \Big] \mathcal{S}. \end{aligned}$$

Here, the times $0 < \tau_1 < \cdots < \tau_n < \beta$ mark the H_2-operator positions, $0 < \tau'_1 < \cdots < \tau'_{n_\sigma} < \beta$ the locations of the bath creation operators, and $0 < \tau''_1 < \cdots < \tau''_{n_\sigma} < \beta$ the locations of the bath annihilation operators ($\sum_\sigma n_\sigma = n$). $\mathcal{S}$ is a permutation sign associated with the separation of the spin-up and -down operators and the grouping of creation and annihilation operators into pairs. Z_c is the partition function for H_1, an irrelevant constant factor that we introduced in order to evaluate the expectation values over the bath states.

The trace over the d-states imposes a constraint on the type of operators we can insert. We can insert either "diagonal operators" $c^\dagger_\sigma c_\sigma$ with σ identical to the spin of the d-Fermion or pairs of spin-flip operators $c^\dagger_\uparrow c_\downarrow$ and $c^\dagger_\downarrow c_\uparrow$. The expectation values $\prod_\sigma \frac{1}{Z_c} \mathrm{Tr}_c[\ldots]$ yield a product of determinants of two matrices, $\det \tilde{M}^{-1}_\uparrow \det \tilde{M}^{-1}_\downarrow$. Due to the scattering term in (8.61), the elements of these matrices are noninteracting Green's functions $\tilde{\mathcal{G}}^\sigma_0$, which are related to the Weiss Green's functions $\mathcal{G}^\sigma_0$ by

$$\tilde{\mathcal{G}}^\sigma_0(i\omega_n) = \frac{\mathcal{G}^\sigma_0(i\omega_n)}{1 + \frac{1}{4} J \mathcal{G}^\sigma_0(i\omega_n)}.$$

Specifically, $[\tilde{M}^{-1}_\sigma]_{ij} = \tilde{\mathcal{G}}^\sigma_0(\tau''_i - \tau'_j)$.

Figure 8.9 shows a possible sequence of operators. The upper two timelines represent the imaginary-time evolution of the spin, and the lower two timelines

https://doi.org/10.1017/CBO9780511902581.009 Published online by Cambridge University Press

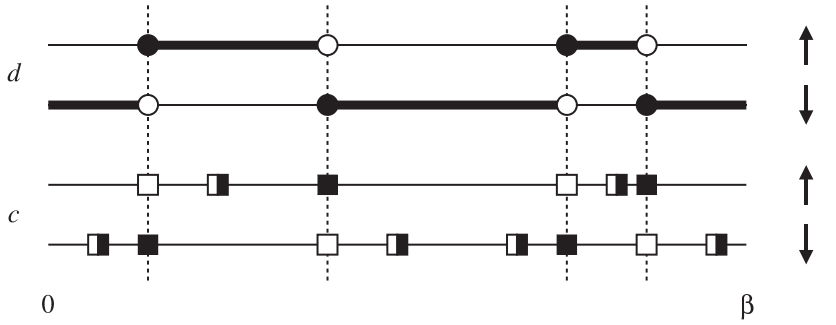

Figure 8.9 Monte Carlo configuration corresponding to four off-diagonal and six diagonal operators. The upper two lines represent the time evolution of the d-states with $\sigma = \uparrow, \downarrow$ (black segments indicate the orientation of the spin s). Full circles represent creation operators and empty circles annihilation operators. A sequence of site 0 creation and annihilation operators for spin up and down is shown on the lower two lines (full and empty squares). The insertion of a diagonal operator $c_\sigma^\dagger(\tau)c_\sigma(\tau)$ is possible only if the spin s is in state σ.

show a sequence of bath creation and annihilation operators. Creation and annihilation operators are represented by full and empty circles or squares. Half-full squares correspond to the diagonal operators $c_\sigma^\dagger(\tau)c_\sigma(\tau)$ whose σ must be identical to the spin represented by the d-line at time τ.

The Monte Carlo sampling proceeds via the insertion and removal of pairs of spin flips (the vertical dashed lines in Fig. 8.9) and via the insertion and removal of diagonal operators (half-filled squares). The spin-flip updates are analogous to the segment configuration updates discussed in Section 8.5.1. We pick a random time for the first spin flip and define an interval $l_{\max}$ up to the next operator, which is either a diagonal operator or a spin-flip event. The second spin flip is then chosen at a random point on this interval. The removal of a pair of adjacent spin flips is possible only if there is no diagonal operator in between. We insert and remove the diagonal operators individually, but an insertion is possible only if the spin is compatible with the state of the d-segment.

The measurement of the bath Green's function at site 0 works just as we described it in the weak-coupling part of Section 8.4.3. This measurement amounts to the accumulation of the T-matrix (see Eq. (8.48))

$$\tilde{t}_\sigma(i\omega_n) = \left\langle -\frac{1}{\beta} \sum_{kl} e^{i\omega_n(\tau_k - \tau_l)} [\tilde{M}_\sigma]_{kl} \right\rangle_{\mathrm{MC}} , \tag{8.62}$$

where the tilde reminds us that this T-matrix is with respect to $\tilde{\mathcal{G}}_0^\sigma$. It is related to the bath Green's function G^σ and the true T-matrix t^σ by

https://doi.org/10.1017/CBO9780511902581.009 Published online by Cambridge University Press

$$G^\sigma(i\omega_n) = \tilde{\mathcal{G}}_0^\sigma(i\omega_n) + \tilde{\mathcal{G}}_0^\sigma(i\omega_n)\tilde{t}^\sigma(i\omega_n)\tilde{\mathcal{G}}_0^\sigma(i\omega_n)$$
$$= \mathcal{G}_0^\sigma(i\omega_n) + \mathcal{G}_0^\sigma(i\omega_n)t^\sigma(i\omega_n)\mathcal{G}_0^\sigma(i\omega_n).$$

Hence, the T-matrix of the bath becomes

$$t^\sigma(i\omega_n) = \frac{-\frac{1}{4}J}{1+\frac{1}{4}J\mathcal{G}_0^\sigma(i\omega_n)} + \frac{\tilde{t}^\sigma(i\omega_n)}{\left[1+\frac{1}{4}J\mathcal{G}_0^\sigma(i\omega_n)\right]^2}, \tag{8.63}$$

and this T-matrix directly yields the impurity Green's function.

8.6.2 Strong-coupling approach

We can also simulate the Kondo impurity model (8.2) efficiently by using the strong-coupling method discussed in Section 8.5. In this approach, we treat the local part of the Hamiltonian,

$$H_{\text{loc}} = -\mu\sum_\sigma c_\sigma^\dagger c_\sigma + J\vec{s}\cdot\left(\frac{1}{2}\psi_c^\dagger\vec{\sigma}\psi_c\right), \tag{8.64}$$

exactly and expand the partition function in powers of the hoppings between the bath orbital 0 (to which the spin s couples) and the rest of the bath (Werner and Millis, 2006). In the chain representation (Fig. 8.8), this hopping amplitude is the parameter V. We integrate out the noninteracting bath sites to obtain an effective action where the eight-dimensional local problem (8.64) is coupled to hybridization functions $\Delta^\sigma(\tau)$ (see Fig. 8.10).

We next diagonalize H_{loc} in a basis labeled by the total number of electrons, the total spin, and the z-component of the total spin. If the particle number is 0 or 2, then the spin state is that of the local moment s. If the number is 1, the spin state is a singlet S or a triplet T_{m_z} with $m_z = 1$, 0, or -1. Accordingly we label the eigenstates as shown in Table 8.1, where the first entry is the number of electrons and the second entry is the spin state. The singlet state S is $(|\uparrow,\downarrow\rangle - |\downarrow,\uparrow\rangle)/\sqrt{2}$ with the first entry being the conduction electron and the second entry the local moment

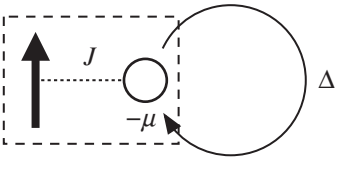

Figure 8.10 Effective action for the Kondo impurity model. The eight-dimensional local problem (dashed box) describes the local spin s coupled to the spin S of the conduction electrons on site 0. The hopping of the conduction electrons from site 0 into the rest of the lattice and back is represented by the hybridization function Δ.

https://doi.org/10.1017/CBO9780511902581.009 Published online by Cambridge University Press

Table 8.1 *Eigenstates and eigenenergies for the local part of the Kondo impurity model (8.64). The first entry labels the number of electrons, and the second entry, the spin state: either impurity spin* $\uparrow, \downarrow$ *if the number of electrons is* 0 *or* 2 *or the total spin S (singlet) or* T_{m_z} *(triplet with* $m_z = 1, 0, -1$*) if* $n = 1$.

Eigenstates	Energy
$\|1\rangle = \|0, \uparrow\rangle$	0
$\|2\rangle = \|0, \downarrow\rangle$	0
$\|3\rangle = \|1, S\rangle$	$-\frac{3}{4}J - \mu$
$\|4\rangle = \|1, T_1\rangle$	$\frac{1}{4}J - \mu$
$\|5\rangle = \|1, T_0\rangle$	$\frac{1}{4}J - \mu$
$\|6\rangle = \|1, T_{-1}\rangle$	$\frac{1}{4}J - \mu$
$\|7\rangle = \|2, \uparrow\rangle$	-2μ
$\|8\rangle = \|2, \downarrow\rangle$	-2μ

spin direction. In this basis, the imaginary-time evolution operator is diagonal, that is, $e^{-H_{\rm loc}\tau}|n\rangle = e^{-E_n\tau}|n\rangle$ with the eigenenergies E_n listed in Table 8.1.

The creation operators for electron spin up and down become the sparse block matrices

$$c_\uparrow^\dagger = \left(\begin{array}{cc|cccc|cc} 0 & 0 & 0 & 0 & 0 & 0 & 0 & 0 \\ 0 & 0 & 0 & 0 & 0 & 0 & 0 & 0 \\ \hline 0 & \frac{1}{\sqrt{2}} & 0 & 0 & 0 & 0 & 0 & 0 \\ 1 & 0 & 0 & 0 & 0 & 0 & 0 & 0 \\ 0 & \frac{1}{\sqrt{2}} & 0 & 0 & 0 & 0 & 0 & 0 \\ 0 & 0 & 0 & 0 & 0 & 0 & 0 & 0 \\ \hline 0 & 0 & \frac{-1}{\sqrt{2}} & 0 & \frac{1}{\sqrt{2}} & 0 & 0 & 0 \\ 0 & 0 & 0 & 0 & 0 & 1 & 0 & 0 \end{array}\right), \tag{8.65}$$

$$c_\downarrow^\dagger = \left(\begin{array}{cc|cccc|cc} 0 & 0 & 0 & 0 & 0 & 0 & 0 & 0 \\ 0 & 0 & 0 & 0 & 0 & 0 & 0 & 0 \\ \hline \frac{-1}{\sqrt{2}} & 0 & 0 & 0 & 0 & 0 & 0 & 0 \\ 0 & 0 & 0 & 0 & 0 & 0 & 0 & 0 \\ \frac{1}{\sqrt{2}} & 0 & 0 & 0 & 0 & 0 & 0 & 0 \\ 0 & 1 & 0 & 0 & 0 & 0 & 0 & 0 \\ \hline 0 & 0 & 0 & -1 & 0 & 0 & 0 & 0 \\ 0 & 0 & \frac{-1}{\sqrt{2}} & 0 & \frac{-1}{\sqrt{2}} & 0 & 0 & 0 \end{array}\right). \tag{8.66}$$

https://doi.org/10.1017/CBO9780511902581.009 Published online by Cambridge University Press

The horizontal and vertical lines define the block structure corresponding to the conservation of the total number of electrons. With these sparse operator matrices, the sampling then proceeds as described in Section 8.5.3, and the measurement procedure for the bath Green's function at site 0 is identical to that described in Section 8.5.2. We finally extract the T-matrix from $G^\sigma(i\omega_n) = \mathcal{G}_0^\sigma(i\omega_n) + \mathcal{G}_0^\sigma(i\omega_n)t^\sigma(i\omega_n)\mathcal{G}_0^\sigma(i\omega_n)$, with $\mathcal{G}_0^\sigma(i\omega_n)$ defined in (8.15), and obtain the impurity Green's function.

While the weak-coupling approach is efficient in the regime of small J, the strong-coupling approach easily captures the singlet-formation occurring at larger J.

8.7 Determinant structure and sign problem

8.7.1 Combination of diagrams into a determinant

The determinants appearing both in the weak- and strong-coupling impurity solvers are a consequence of Wick's theorem for the noninteracting part of the Hamiltonian (weak-coupling approach) or the noninteracting bath (strong-coupling approach). In a manner similar to what we saw in Section 7.1.2, a determinant of an $n \times n$ matrix corresponds to a collection of $n!$ diagrams for the partition function. In this collection, both connected and disconnected diagrams appear. What the $n!$ diagrams have in common are the positions on the imaginary-time interval of the n interaction vertices (weak-coupling approach) or the positions of the n creation and n annihilation operators (strong-coupling approach). Figure 8.11 illustrates all second-order

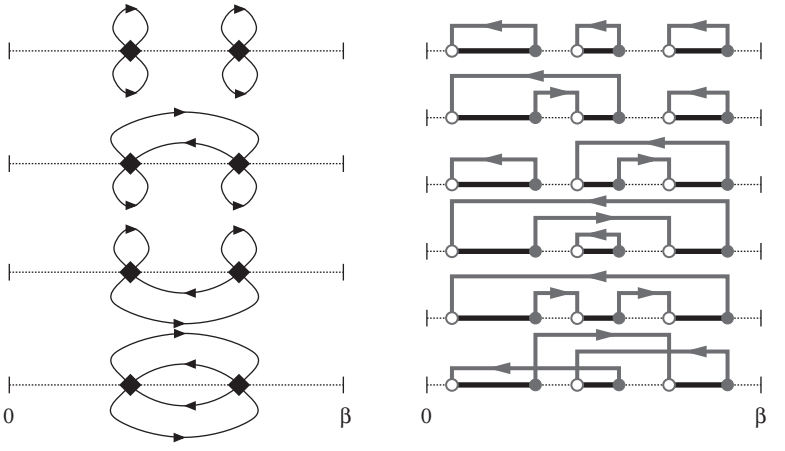

Figure 8.11 Left panel: weak-coupling diagrams summable into a determinant. The diamonds represent interaction vertices and the lines Weiss Green's functions for spin-up and -down electrons. Right panel: strong-coupling diagrams summable into a determinant. The empty circles represent creation operators and the full circles annihilation operators. Pairs of creation and annihilation operators are connected by hybridization lines.

https://doi.org/10.1017/CBO9780511902581.009 Published online by Cambridge University Press

(weak-coupling) and third-order (strong-coupling) contributions corresponding to some fixed operator positions. We note that the Fermionic nature of the operators leads to individual diagrams with anticommutivity signs. The determinants allow us to sum up $n!$ diagrams with proper signs and, at least in simple models such as the Anderson impurity model, to completely absorb the cancellation effects between positive and negative weight contributions.

To underscore the crucial role of the determinants, we consider a simple model of a noninteracting (spin-less) impurity coupled to one bath site with energy $\varepsilon = 0$ and hybridization V. The action reads

$$S = \int_0^\beta d\tau \int_0^\beta d\tau' \, d^\dagger(\tau')\Delta(\tau' - \tau)d(\tau),$$

with the hybridization function (8.14) given by $\Delta(i\omega_n) = |V|^2/i\omega_n$, which in imaginary time becomes

$$\Delta(\tau) = \begin{cases} -\frac{1}{2}|V|^2 & 0 < \tau < \beta, \\ \frac{1}{2}|V|^2 & -\beta < \tau < 0. \end{cases}$$

In this simple model, the absolute values of the diagram weights depend only on the perturbation order n and not on the operator positions, so the integral over the operator positions merely produces a factor $2\beta^{2n}/(2n)!$. The combined weight of the $n!$ topologically distinct diagrams corresponding to a set of n creation and n annihilation operators is the determinant

$$\det \begin{pmatrix} \frac{1}{2}|V|^2 & \frac{1}{2}|V|^2 & \frac{1}{2}|V|^2 & \dots \\ -\frac{1}{2}|V|^2 & \frac{1}{2}|V|^2 & \frac{1}{2}|V|^2 & \dots \\ -\frac{1}{2}|V|^2 & -\frac{1}{2}|V|^2 & \frac{1}{2}|V|^2 & \dots \\ \vdots & \vdots & \vdots & \ddots \end{pmatrix} = \frac{1}{2}|V|^{2n}, \tag{8.67}$$

when we take into account the signs from the time ordering. This means that in the Monte Carlo sampling based on determinants, there is no sign problem and configurations with order n are generated with a probability

$$p_{\text{determinants}}(n) \sim (\beta|V|)^{2n}/(2n)!.$$

On the other hand, the probability distribution obtained in a sampling of individual diagrams (based on the absolute value of their weights) is

$$p_{\text{diagrams}}(n) \sim (n!/2^n)(\beta|V|)^{2n}/(2n)!.$$

Figure 8.12 compares these two distribution functions for inverse temperatures $\beta|V| = 2$ and $\beta|V| = 20$. At the lower temperature, a simulation based on a sampling of individual diagrams would spend most of the time generating configurations of order ~ 50. However, as the distribution for the determinants shows,

https://doi.org/10.1017/CBO9780511902581.009 Published online by Cambridge University Press

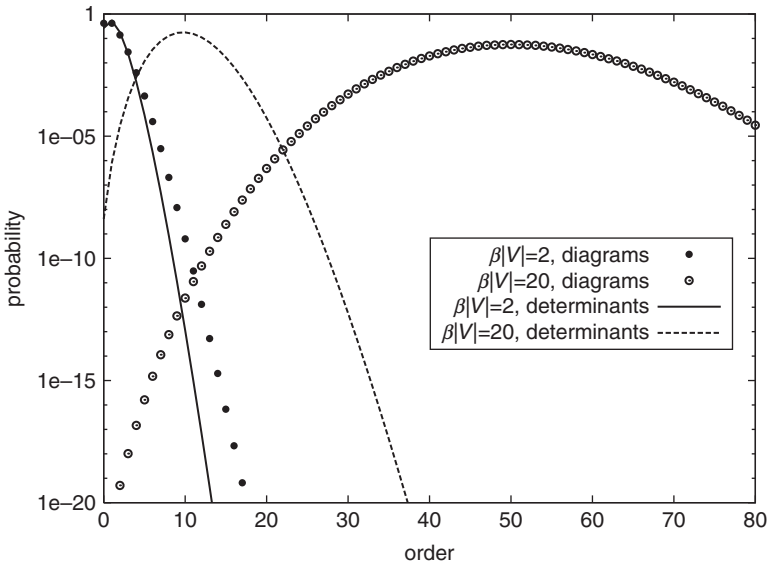

Figure 8.12 Perturbation order distribution (per spin) for the noninteracting Anderson impurity model with one bath site (energy $\varepsilon = 0$, hybridization V, inverse temperature β). The circles show the distribution obtained in a sampling of individual strong-coupling diagrams, while the lines show the distribution in the sampling of determinants.

these configurations contribute negligibly to the partition function (and hence to physical observables) due to sign cancellations. The perturbation orders that are actually relevant are much lower, as the distribution function for the determinants peaks at order ~ 10. There are thus two related reasons why the summation of diagrams into determinants is so important, especially at low temperature:

1. The determinants sum an enormous number of individual diagrams. The determinant of a 100×100 matrix is easily computed numerically and corresponds to the combined weight of $100! = 10^{158}$ diagrams! In practice we can treat average perturbation orders up to ~ 1000.
2. The determinant-based sampling generates configurations with lower perturbation orders than a sampling of individual diagrams. This gain in efficiency is the result of sign cancellations between high-order diagrams.

8.7.2 Absence of a sign problem

To prove the absence of a sign problem in the weak- and strong-coupling continuous-time Monte Carlo simulation of the Anderson impurity model, we use the chain

https://doi.org/10.1017/CBO9780511902581.009 Published online by Cambridge University Press

representation of the impurity model introduced in Section 8.1.1. We first discuss the weak-coupling approach (Yoo et al., 2005), assuming that the interaction term is rewritten according to (8.31) and (8.32). In the chain representation the quadratic part of the Hamiltonian is

$$\tilde{H}_0 = \sum_{\sigma} \sum_{j=0}^{\infty} \left[\tilde{\varepsilon}_j c_{j\sigma}^{\dagger} c_{j\sigma} - t_j (c_{j+1,\sigma}^{\dagger} c_{j\sigma} + c_{j\sigma}^{\dagger} c_{j+1,\sigma}) \right].$$

Here, c_j is the annihilation operator for site j of the chain, $c_0 \equiv d$, $t_0 \equiv V$, and $\tilde{\varepsilon}_0 = -\mu + \frac{1}{2}U$ (see Fig. 8.1). We choose the chain basis such that all hopping parameters t_j are nonnegative. By adding an appropriate term $\Lambda(N_\uparrow + N_\downarrow)$, with $\Lambda \geq 0$ and $N_\sigma = \sum_j c_{j\sigma}^{\dagger} c_{j\sigma}$, we further ensure that all diagonal elements of $\tilde{H}_0 - \Lambda(N_\uparrow + N_\downarrow)$ are negative or zero. Hence, all elements of the matrix $\exp[-(\tilde{H}_0 - \Lambda(N_\uparrow + N_\downarrow))]$ are positive or zero in the chain basis. Since $\tilde{H}_0$ conserves N_σ,

$$e^{-\tau \tilde{H}_0} = e^{-\tau(\tilde{H}_0 - \Lambda(N_\uparrow + N_\downarrow))} e^{-\tau \Lambda (N_\uparrow + N_\downarrow)}$$

is a product of two matrices with elements ≥ 0, and therefore the time-evolution operator has no negative elements in the chain basis.

The weight of a weak-coupling Monte Carlo configuration is

$$w_C = \mathrm{Tr} \left[e^{-(\beta - \tau_n)\tilde{H}_0} A(s_n) e^{-(\tau_n - \tau_{n-1})\tilde{H}_0} A(s_{n-1}) \cdots \right] (d\tau)^n,$$

where

$$A(s) = (-U/2) \left[n_\uparrow - \tfrac{1}{2} - s(\tfrac{1}{2} + \delta) \right] \left[n_\downarrow - \tfrac{1}{2} + s(\tfrac{1}{2} + \delta) \right].$$

What we still need to show is that the matrix $A(s)$ has only nonnegative elements when $\delta \geq 0$ and $U \geq 0$. We do this by considering the two values of the auxiliary spin variable s and by factorizing the interaction term into a product of two diagonal operators:

$$\begin{aligned} s = 1 &: \underbrace{(-U/2)}_{\leq 0} \underbrace{(n_\uparrow - 1 - \delta)}_{\leq 0} \underbrace{(n_\downarrow + \delta)}_{\geq 0}, \\ s = -1 &: \underbrace{(-U/2)}_{\leq 0} \underbrace{(n_\uparrow + \delta)}_{\geq 0} \underbrace{(n_\downarrow - 1 - \delta)}_{\leq 0}. \end{aligned}$$

Hence, in the chain basis, neither the imaginary-time evolution operators $e^{-\tau \tilde{H}_0}$ nor the "interaction vertices" $A(s)$ have negative elements. The weight is the trace of a product of matrices with nonnegative elements, and therefore must be nonnegative. We recall that in the case of attractive U, no auxiliary-field decoupling is required, and the weak-coupling weights are evidently positive.

The lack of a sign problem proof for the strong-coupling formalism is also based on the chain basis (Kaul, 2007). Here, the weight of a Monte Carlo configuration has the form

https://doi.org/10.1017/CBO9780511902581.009 Published online by Cambridge University Press

$$w_C = \mathrm{Tr}\Big[e^{-(\beta-\tau_n)(H_{\mathrm{loc}}+H_{\mathrm{bath}})}(-H_{\mathrm{mix}}^{d^\dagger}) \cdots e^{-(\tau_2-\tau_1)(H_{\mathrm{loc}}+H_{\mathrm{bath}})}(-H_{\mathrm{mix}}^{d}) e^{-\tau_1(H_{\mathrm{loc}}+H_{\mathrm{bath}})}\Big](d\tau)^{2n}, \tag{8.68}$$

with $-H_{\mathrm{mix}}^{d^\dagger} = Vc_0^\dagger c_1$, $-H_{\mathrm{mix}}^{d} = Vc_1^\dagger c_0$ ($c_0 \equiv d$). In the chain basis, the hybridization operators do not produce any negative signs ($V \geq 0$).[23] In the imaginary-time evolution operators, H_{loc} is diagonal, while H_{bath} has off-diagonal elements $-t_i \leq 0$ ($i = 1, 2, \ldots$). Writing

$$e^{-\tau(H_{\mathrm{loc}}+H_{\mathrm{bath}})} = \lim_{N\to\infty}\left(I - \frac{\tau}{N}[H_{\mathrm{loc}} + H_{\mathrm{bath}}]\right)^N,$$

we see that inside the parentheses on the right-hand side the diagonal terms (dominated by 1) are positive, and the off-diagonal terms (originating from $-\frac{\tau}{N}H_{\mathrm{bath}}$) are nonnegative. Hence, the imaginary-time evolution operator has no negative elements. The Monte Carlo weights are therefore also the trace of a product of matrices with nonnegative elements.

8.8 Scaling of the algorithms

In the weak- and strong-coupling algorithms, the average expansion orders have a simple physical interpretation. In a DMFT calculation, they yield highly accurate measurements for the potential and kinetic energy.

Let us first consider the weak-coupling algorithm, where after the introduction of auxiliary fields (Equations (8.31) and (8.32)) and the shifting of the chemical potential $H = H_1 + H_2$, with $H_1 = H_\mu + \frac{1}{2}U(n_\uparrow + n_\downarrow) + H_{\mathrm{bath}}$ and $H_2 = Un_\uparrow n_\downarrow - \frac{1}{2}U(n_\uparrow + n_\downarrow)$.[24] It follows from (8.29) that

$$\begin{aligned}
\langle -H_2\rangle &= \frac{1}{\beta}\int_0^\beta d\tau \langle -H_2(\tau)\rangle \\
&= \frac{1}{\beta}\frac{1}{Z}\sum_{n=0}^{\infty}\frac{n+1}{(n+1)!}\int_0^\beta d\tau \int_0^\beta d\tau_1 \cdots \int_0^\beta d\tau_n \\
&\quad \times \mathrm{Tr}\left[e^{-\beta H_1}\mathcal{T}(-H_2(\tau))(-H_2(\tau_n))\cdots(-H_2(\tau_1))\right] \\
&= \frac{1}{\beta}\frac{1}{Z}\sum_C n_C w_C = \frac{1}{\beta}\langle n\rangle,
\end{aligned} \tag{8.69}$$

[23] Here, we don't actually need this sign convention, as these factors come in complex conjugate pairs.
[24] For simplicity, we have chosen $\delta = 0$.

https://doi.org/10.1017/CBO9780511902581.009 Published online by Cambridge University Press

and therefore the average perturbation order $\langle n \rangle$ is related to the potential energy by

$$\langle n \rangle_{\text{weak-coupling}} = -\beta U \langle n_\uparrow n_\downarrow \rangle + \tfrac{1}{2}\beta U \langle n_\uparrow + n_\downarrow \rangle = -\beta E_{\text{pot}} + \tfrac{1}{2}\beta U \langle n_\uparrow + n_\downarrow \rangle. \quad (8.70)$$

We also learn from this formula that the average perturbation order is roughly proportional to the inverse temperature β and the interaction strength U.

In the strong-coupling case, the average perturbation order is proportional to the kinetic energy. In single-site DMFT, we can express the kinetic energy

$$E_{\text{kin}} = \sum_{k\sigma} \epsilon_k G_{k\sigma}(0^-)$$

in terms of the local Green's function and hybridization function:[25]

$$E_{\text{kin}} = \sum_\sigma \int_0^\beta d\tau G_\sigma(\tau) \Delta^\sigma(-\tau).$$

Substituting the strong-coupling measurement formula (8.53) for G into this expression, we find

$$\begin{aligned} E_{\text{kin}} &= \sum_\sigma \int_0^\beta d\tau \left\langle -\sum_{ij} \frac{1}{\beta} \delta(\tau, \tau_i - \tau_j')[M_\sigma]_{ij} \right\rangle_{\text{MC}} \Delta^\sigma(-\tau) \\ &= -\sum_\sigma \left\langle \frac{1}{\beta} \sum_{ij} [M_\sigma]_{ij} \Delta^\sigma(\tau_j' - \tau_i) \right\rangle_{\text{MC}}. \end{aligned}$$

[25] The first step in the derivation of this formula is to switch to the Fourier representation:

$$\begin{aligned} E_{\text{kin}} &= \sum_{k\sigma} \epsilon_k G_{k\sigma}(0^-) = \sum_{k\sigma} \epsilon_k \frac{1}{\beta} \sum_n e^{-i\omega_n 0^-} G_{k\sigma}(i\omega_n) \\ &= \sum_{k\sigma} \epsilon_k \frac{1}{\beta} \sum_n e^{i\omega_n 0^+} \frac{1}{i\omega_n + \mu - \epsilon_k - \Sigma_\sigma(i\omega_n)}. \end{aligned}$$

Introducing the density of states $\mathcal{D}(\varepsilon)$, we can then write

$$\begin{aligned} E_{\text{kin}} &= \sum_\sigma \frac{1}{\beta} \sum_n e^{i\omega_n 0^+} \int d\epsilon \frac{\epsilon}{i\omega_n + \mu - \epsilon - \Sigma_\sigma(i\omega_n)} \mathcal{D}(\epsilon) \\ &= \sum_\sigma \frac{1}{\beta} \sum_n e^{i\omega_n 0^+} \int d\epsilon \frac{-[i\omega_n + \mu - \epsilon - \Sigma_\sigma(i\omega_n)] + [i\omega_n + \mu - \Sigma_\sigma(i\omega_n)]}{i\omega_n + \mu - \epsilon - \Sigma_\sigma(i\omega_n)} \mathcal{D}(\epsilon) \\ &= \sum_\sigma \frac{1}{\beta} \sum_n e^{i\omega_n 0^+} (-1 + [i\omega_n + \mu - \Sigma_\sigma(i\omega_n)] G^\sigma_{\text{loc}}(i\omega_n)), \end{aligned}$$

with G_{loc} the local lattice Green's function, which after convergence of the DMFT calculation is identical to the impurity Green's function G. The latter is related to the hybridization function by $G = [i\omega_n + \mu - \Sigma - \Delta]^{-1}$. Hence, we obtain

$$E_{\text{kin}} = \sum_\sigma \frac{1}{\beta} \sum_n e^{i\omega_n 0^+} G_\sigma(i\omega_n) \Delta^\sigma(i\omega_n) = \sum_\sigma \int d\tau G_\sigma(\tau) \Delta^\sigma(-\tau).$$

https://doi.org/10.1017/CBO9780511902581.009 Published online by Cambridge University Press

Now we use that $[M_\sigma]_{ij} = (-1)^{i+j} \det M_\sigma^{-1}[j,i] / \det M_\sigma^{-1}$, where $\det M_\sigma^{-1}[j,i]$ denotes the hybridization matrix with row j and column i removed. Hence, the sum

$$\sum_j (-1)^{i+j} \det M_\sigma^{-1}[j,i] \Delta^\sigma(\tau_j' - \tau_i) = \det M_\sigma^{-1}$$

appearing in the nominator is nothing but the expansion of the determinant of the hybridization matrix along column i. The expression for the kinetic energy thus simplifies to

$$E_{\text{kin}} = -\sum_\sigma \left\langle \frac{1}{\beta} \sum_i \frac{\det M_\sigma^{-1}}{\det M_\sigma^{-1}} \right\rangle_{\text{MC}} = -\frac{1}{\beta} \sum_\sigma \langle n_\sigma \rangle ,$$

and the average total perturbation order $\langle n \rangle$ of the Monte Carlo configuration is related to the kinetic energy by

$$\langle n \rangle_{\text{strong-coupling}} = -\beta E_{\text{kin}}.$$

While the average expansion order in both the weak- and strong-coupling methods scales as β, the scaling of the expansion order with the interaction strength is very different. In the weak-coupling approach it grows roughly proportional to U, while in the strong-coupling approach, it decreases with increasing U (Fig. 8.13). In the case of the Anderson impurity model, this behavior leads to a significant computational speed-up for the strong-coupling approach in the intermediate- and

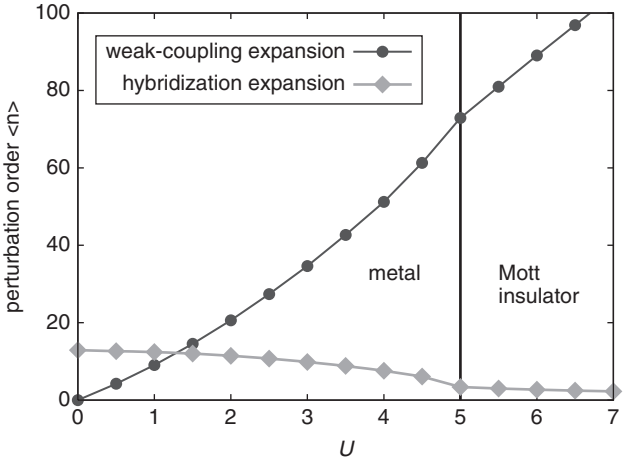

Figure 8.13 Average perturbation order for the weak-coupling and strong-coupling (hybridization expansion) algorithms. These results correspond to the DMFT solution of the one-band Hubbard model with semicircular density of states of bandwidth 4 and temperature $T = 1/30$. The bath is therefore different for each data point. (Figure adapted from Gull et al. (2007).)

https://doi.org/10.1017/CBO9780511902581.009 Published online by Cambridge University Press

Table 8.2 *Scaling of the different impurity solvers with inverse temperature β and system size L. In the case of the segment algorithm, we assume that the calculation of the determinant ratios dominates the overlap calculations. In the matrix or Krylov case, we assume that the trace calculation dominates the calculation of the determinant ratios.*

Solver	Scaling		Use
Weak-coupling	β^3	L^3	Impurity clusters with density-density interaction
Hybridization expansion (segment formalism)	β^3	L	Single-site multi-orbital models with density-density interaction
Hybridization expansion (matrix/Krylov formalism)	β	$\exp(L)$	Single-site multi-orbital models with general U_{ijkl}

large-U regime. Since local updates are $\mathcal{O}(n^2)$, a full sweep (update of all vertices in a configuration) is order $\mathcal{O}(n^3)$.

For impurity clusters, or models with complicated interaction terms, which require the matrix or Krylov formalisms discussed in Sections 8.5.3 and 8.5.4, the strong-coupling method scales exponentially with system size, and we can apply it only to relatively small systems. Here, the weak-coupling approach, if applicable, can be the method of choice. Table 8.2 gives a summary of the different scalings (assuming a diagonal hybridization) and indicates which solver is appropriate for which type of problem. The weak-coupling solvers are mainly used in cluster DMFT or DCA calculations of the Hubbard model, where the polynomial scaling allows us to treat clusters of up to 100 sites (Fuchs et al., 2011), at least in parameter regimes where there is no serious sign problem. The strong-coupling approach, on the other hand, is useful in particular for the study of (single-site) multi-orbital problems with complicated local interactions. Such problems typically have to be solved in single-site DMFT studies of strongly correlated materials or in realistic simulations of transition metal impurities (Surer et al., 2012).

Suggested reading

A. Georges, G. Kotliar, W. Krauth, and M. J. Rozenberg, "Dynamical mean-field theory of strongly correlated Fermion systems and the limit of infinite dimensions," *Rev. Mod. Phys.* **68**, 13 (1996).

A. Georges, "Strongly Correlated Electron Materials: Dynamical Mean-Field Theory and Electronic Structure," in *Lectures on the Physics of Highly Correlated Electron Systems VIII*, ed. A. Avella and F. Mancini, AIP Conference Proceedings, **715**, (2004).

T. Maier, M. Jarrell, T. Pruschke, and M. H. Hettler, "Quantum cluster theories," *Rev. Mod. Phys.* **77**, 1027 (2005).

G. Kotliar, S. Y. Savrasov, K. Haule, V. S. Oudovenko, O. Parcollet, and C. A. Marianetti, "Electronic structure calculations with dynamical mean-field theory," *Rev. Mod. Phys.* **78**, 865 (2006).

E. Gull, A. J. Millis, A. L. Lichtenstein, A. N. Rubtsov, M. Troyer, and P. Werner, "Continuous-time Monte Carlo methods for quantum impurity models," *Rev. Mod. Phys.* **83**, 349 (2011).

Exercises

8.1 Consider the semi-infinite spinless Fermion chain with Hamiltonian

$$H = \sum_{j=0}^{\infty} \left[\varepsilon_j c_j^\dagger c_j - t_j^* c_j^\dagger c_{j+1} - t_j c_{j+1}^\dagger c_j \right] \tag{8.71}$$

in a site representation. For $j \geq 1$, we define the gauge transformed operators $\tilde{c}_j$ by $c_j = \exp[i \sum_{k<j} \varphi_j] \tilde{c}_j$, where φ_j is the phase of t_j ($t_j = |t_j| e^{i\varphi_j}$). Show that in terms of the transformed operators, the Hamiltonian becomes ($c_0 \equiv \tilde{c}_0$)

$$H = \sum_{j=0}^{\infty} \left[\varepsilon_j \tilde{c}_j^\dagger \tilde{c}_j - |t_j| \tilde{c}_j^\dagger \tilde{c}_{j+1} - |t_j| \tilde{c}_{j+1}^\dagger \tilde{c}_j \right], \tag{8.72}$$

which means that all hopping terms are nonnegative.

8.2 Using the fast-update formula (8.39) for determinant ratios, derive the measurement formula (8.46) for the Green's function in the weak-coupling algorithm.

8.3 Show that the Matsubara transform of the β-antiperiodic constant function

$$\Delta(\tau) = \begin{cases} -\frac{1}{2}|V|^2 & 0 < \tau < \beta \\ \frac{1}{2}|V|^2 & -\beta < \tau < 0 \end{cases} \tag{8.73}$$

is $\Delta(i\omega_n) = |V|^2 / i\omega_n$. Prove (8.67) by induction.

8.4 Show that the function

$$\Delta(\tau) = \sum_p \frac{|V_p|^2}{e^{\varepsilon_p \beta} + 1} \begin{cases} -e^{-\varepsilon_p(\tau-\beta)} & 0 < \tau < \beta \\ e^{-\varepsilon_p \tau} & -\beta < \tau < 0 \end{cases} \tag{8.74}$$

is β-antiperiodic and compute its Matsubara transform; that is, derive the formula $\Delta(i\omega_n) = \sum_p |V_p|^2 / (i\omega_n - \varepsilon_p)$.

8.5 By taking into account the Fermionic anticommutivity signs, verify for perturbation orders 1, 2, and 3 that the weights of all the weak-coupling diagrams corresponding to a fixed position of the interaction vertices can be summed up into a determinant.

https://doi.org/10.1017/CBO9780511902581.009 Published online by Cambridge University Press

8.6 Verify that the weights of the six strong-coupling diagrams shown in the right-hand panel of Fig. 8.11 sum to a determinant. For a time-independent hybridization function of the form (8.73), show that the weights of the first five diagrams are positive, while the weight of the last diagram is negative. Connect this observation to the number of crossing hybridization lines.

8.7 For the local Hamiltonian H_{loc} of the Anderson impurity model and Kondo impurity model, write down the eigenstates and group them according to conserved quantum numbers.

8.8 In DCA, the cluster hybridization function Δ_K is related to the bath Green's function $\mathcal{G}_{0,K}$ by

$$i\omega_n + \mu - \bar{\epsilon}_K - \Delta_K(i\omega_n) = \mathcal{G}_{0,K}^{-1}(i\omega_n), \tag{8.75}$$

where $\bar{\epsilon}_K$ is the average of the dispersion ϵ_k over momentum patch K. Prove this relation by calculating the high-frequency expansion of $\mathcal{G}_{0,K}^{-1}(i\omega_n) = (G_{\text{imp}}^K)^{-1}(i\omega_n) + \Sigma^K(i\omega_n)$, using (8.25), and by imposing $\Delta_K(i\omega_n) \propto \frac{1}{i\omega_n} + O(\frac{1}{(i\omega_n)^2})$. The latter condition ensures that the hybridization function has no instantaneous hopping-type contribution.

https://doi.org/10.1017/CBO9780511902581.009 Published online by Cambridge University Press